Accounts

Photochemistry for the Synthesis of Noble Metal Nanoparticles

Masanori Sakamoto and Tetsuro Majima*

The Institute of Scientific and Industrial Research (SANKEN), Osaka University,
8-1 Mihogaoka, Ibaraki, Osaka 567-0047

Received April 5, 2010; E-mail: majima@sanken.osaka-u.ac.jp

The synthesis of metal nanoparticles is an interdisciplinary subject that is attracting intense research and development owing to the fundamental scientific value of nanometer-sized metal, as well as the broad range of potential applications of metal nanoparticles. Photochemistry plays an important role in various aspects of this research area. It is a unique tool for synthesizing metal nanoparticles, as well as an important technique for investigating the formation mechanism. Metal nanoparticles formation triggered by photochemical reaction is effective for investigating formation mechanisms. We succeeded in observing the formation of metal nanoparticles and clusters by using spectroscopic methods. In addition, single-molecule fluorescent spectroscopy provided important insights into the photochemical reactivity of metal clusters. This photochemical reactivity offers a promising possibility with regard to metal clusters. We developed strategies for constructing metal nanoparticles using a series of photochemical techniques. In situ photochemical synthesis is an effective method for the fabrication of metal nanoparticles, as well as composite materials. A multicolor excitation-induced photochemical reaction resulted in the reduction of metal ions with a highly negative reduction potential, recyclable photosensitization, and 3-D direct laser writing of metal nanoparticles. These new strategies will expand the possible applications of photochemistry for metal nanoparticles synthesis.

Introduction

The synthesis of metal nanoparticles (NPs) is a research subject that has achieved spectacular breakthroughs in recent decades. The intense investigation and research currently in progress reflect the fundamental scientific interest in nanometer-sized metals, as well as the specific optical, electrical, and catalytic properties of nanometer-sized metals, which show promise for a wide range of applications spanning the fields of catalysis, electronics, photonics, imaging, and therapy.[1–13]

The development of a method for the synthesis of metal NPs is a subject of interdisciplinary research spanning multiple scientific domains. Almost every conceivable approach to synthesis has been attempted, including chemical, photochemical, radiation chemical, mechanochemical, biochemical, and thermal methods.[14–24] Photochemistry plays an important role in various aspects of this research. It is a powerful tool in the synthesis of metal NPs, as well as an important technique for investigating the mechanism of their formation.

The photochemical synthetic method generates metal atom (M^0) through the direct photoreduction of a metal source (metal salt or complex), or the reduction of metal ions using photochemically generated intermediates such as excited molecules and radicals (photosensitization) (Scheme 1). Although the principle of the photochemical method is based on a bottom up strategy, the advantages and direction of its application are critically different from other bottom up methods. For example, photochemical synthesis has been applied to photography (photographically sensitive materials use silver salt) and lithography, because photochemical synthesis is suitable for the selective fabrication of metal NPs with high spatial resolution.[16,25–29] On the other hand, most methods of synthesis of metal NPs do not have this feature.

The utilization of photochemistry is mainly responsible for the unique characteristics of the photochemical method. In other words, *what makes the photochemical synthesis different from other methods is the character of light, which controls photochemical reactions*. The characteristic advantages of the photochemical synthesis of metal NPs are summarized as follows.

High Spatial Resolution. As can be seen in photography and photolithography, light-induced processing has high spatial resolution. Owing to this advantage, the photochemical synthetic methods can fabricate metal NPs in a selected and microscopic region.[16,25–29] The three-dimensional (3-D) resolution offers another critical advantage. The direct 3-D writing of metal NPs in a transparent matrix or free standing metal structures has been achieved using multiphoton absorption with an ultrashort-pulse laser, or through stepwise excitation using two laser beams of different wavelengths.[28,30–36]

Fine photoprocessing has long been fraught with the problem of diffraction limits. Currently however, a number of

Published on the web October 5, 2010; doi:10.1246/bcsj.20100097

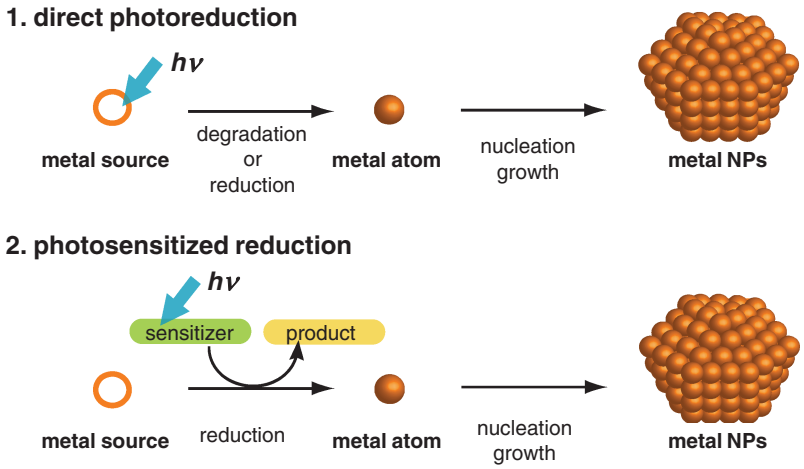

Scheme 1. Systematic scheme of photo-induced synthesis of metal NPs.

solutions have been advanced to overcome this problem, such as processing using nonlinear optical phenomena, evanescent wave, or two-laser beams of different wavelengths.[33,37–43]

Reaction Selectivity. The first law of photochemistry states that *light must be absorbed by a chemical substance in order for a photochemical reaction to take place*. Due to this law, light can simulate an objective reaction without affecting the external circumstances. This advantage is useful for the in situ fabrication of metal NPs in transparent matrices, as well as the template synthesis of metal NPs using micelles, biological molecules, zeolite, dendrimer, etc.[44–46]

Reaction Controllability. Understanding of the formation and growth mechanisms of metal NPs is essential for the development of synthesis of metal NPs that have the desired physical properties. Light is the exclusive trigger of a photochemical reaction and this characteristic allows us to start the formation of metal NPs through photochemical reaction at any given point in time. Photochemistry is therefore a powerful tool for investigating the formation and growth processes of metal NPs.

Shape Conversion via Photoirradiation. Photochemical reaction can tune the size and shape of generated metal NPs.[47–52] In addition, the light irradiation to NPs often causes a change in their size and/or shape.[53–58] For this reason, light can be utilized to regulate the size and shape of metal NPs, as well as the fabrication of metal NPs. The light-induced conversion of Ag NPs to nanoprisms is one remarkable example, which demonstrates the light-induced regulation of the size and shape of metal NPs.[54,56,58]

In this account, we review our recent research and discuss the role and potential of photochemistry in the synthesis of metal NPs. We begin by investigating the primal step in the formation of metal NPs, that is, the formation and growth processes of Au clusters and their photochemical reactivity (Section **1**).[59,60] Then, we show the in situ photochemical fabrication of larger Au NPs and core/shell NPs in polymer film (Section **2**). In Section **3**, we describe the development of a new method of photochemical synthesis using multiple laser beams of different wavelengths. The 3-D writing of metal NPs using multiple laser beams is described in Section **4**. Finally, we summarize our research and discuss future avenues for the photochemistry in the synthesis of metal NPs.

1. Photochemical Fabrication of a Noble Metal Cluster

In the case of the bottom-up synthesis of metal NPs, the M^0 are associated to form small clusters that then grow to be larger NPs. The formation process of metal clusters is a subject of great importance for better understanding of the primal stage of metal NPs formation. In addition, the characteristics of metal clusters, which are composed of several tens of atoms, have attracted considerable attention for a variety of reasons, ranging from a fundamental scientific interest in nanoscopic materials to their technological applications.[8,61–73]

Au NPs of 5–20 nm in diameter show a surface plasmon band owing to the characteristic collective oscillation frequency of freely mobile electrons in NPs. Upon excitation, the plasmon oscillations relax nonradiatively via collisions of electron–electron, electron–lattice phonon, and electron–surface. On the contrary, Au clusters smaller than 2.2 nm in diameter exhibit molecule-like transitions because of the discretization of the density of states.[8,60–62] The discrete states of noble-metal clusters, along with their fluorescence, invite an investigation into the behavior and reactivity of these metal clusters using spectroscopic techniques. Single-molecule fluorescence spectroscopy (SMS) is a powerful method that can reach the individual clusters underlying the heterogeneous characteristics of materials.[74] We fabricated Au clusters using a photochemical method in a polymer matrix and concurrently investigated the formation process and photoreactivity of clusters generated at the single-cluster level.[75,76] This approach allowed us to achieve a better understanding of the following subjects of interest. (1) The fluorescence spectra of metal clusters were characterized by the number of atoms, thus allowing the identification of atom numbers of metal cluster samples during growth. The study provided new insight into the growth process of clusters, and the synthesis of metal clusters with a strict limitation on the number of atoms. (2) Due to the molecular-like transitions involved, the photochemical reactivity of quantized metal is a subject of great interest. Our SMS investigation of Au clusters fabricated in polymer film allowed us to understand the photochemical reactivity of ligand-free Au clusters.

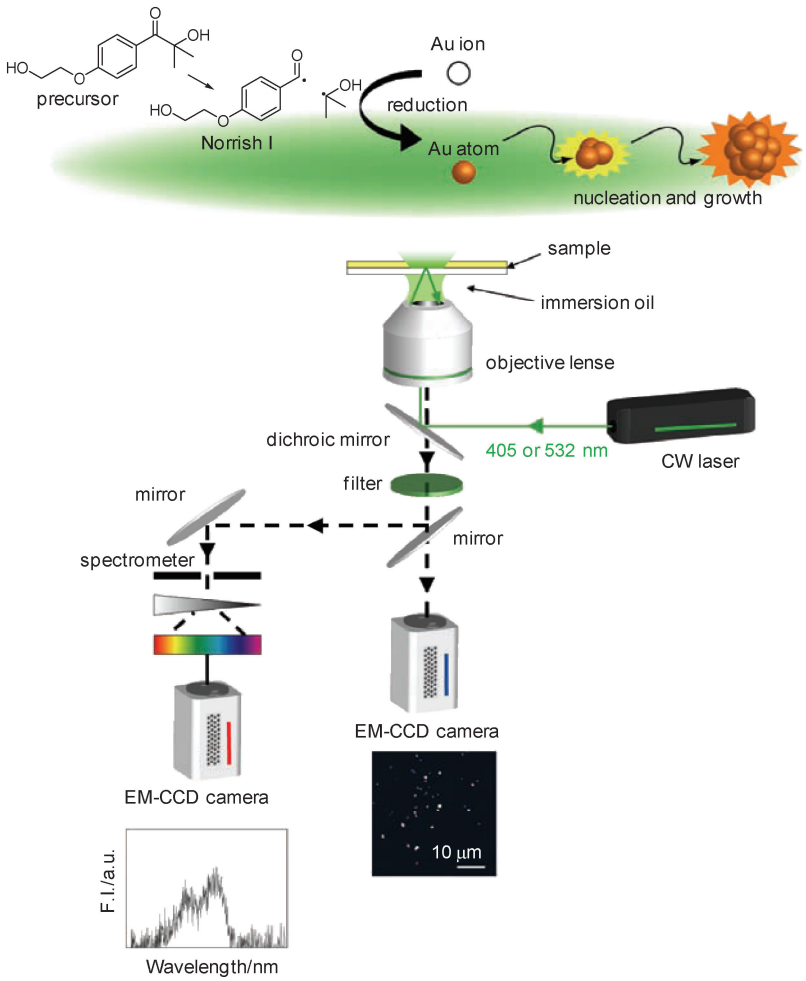

Scheme 2. Formation and growth processes of Au clusters in a polymer film (upper illustration). Experimental setup for single molecule fluorescence microscopy (lower illustration).[77]

1.1 Formation and Growth Processes of Au Clusters. The formation mechanism of Au clusters is shown in Scheme 2. A poly(vinyl acetate) (PVAc) film containing a radical precursor [2-hydroxy-4′-(2-hydroxyethoxy)-2-methylpropiophenone] and $H[AuCl_4]$ (denoted as **PVAc**) was prepared. PVAc can disperse and stabilize Au clusters. Upon photoexcitation, the radical precursor yields radicals via a Norrish-type-I α-cleavage.[16] These radicals work as reducing agents for the Au ion in order to generate an Au atom. Figure 1A shows the absorption spectra of bulk **PVAc** before and after UV-light irradiation. It can be observed that the broad absorption band at 420 nm appeared after irradiation. The UV-light-irradiated **PVAc** matrix exhibited luminescence with excitation and emission maxima at 409 and 490 nm, respectively, indicating the formation of Au clusters (Au_n, n = atom number) (Figure 1B).

When the UV-irradiated **PVAc** film (i.e., Au_n) was stored in the dark for a sufficient period of time (aging), a new peak appeared at 542 nm (Figure 1A), and the color of emission turned to vivid pink (Figure 1C). Following this change in the absorption spectrum, the emission peak at 490 nm decreased, and a new emission appeared at the longer wavelength (Figure 1D). The newly observed emission showed excitation and emission spectra maxima at 550 and 583 nm, respectively (Figure 1B). A transmission electron microscopy (TEM) image revealed that the average diameter of the Au clusters increased from 1.0 to 1.5 nm during aging (Figures 1E and 1F). The absorption spectrum of aged-**PVAc** film can be assigned to the molecule-like transition of clusters because AuNPs with a diameter less than 3 nm do not show the surface plasmon band. This indicates that the changes in the absorption and fluorescence spectra of the **PVAc** film were caused by the formation of new Au clusters with a larger number of atoms, Au_m ($m > n$).

The experimental setup for the direct observation of the formation and growth processes of a single Au cluster is illustrated in Scheme 2. The **PVAc** thin film was irradiated with a 405-nm diode laser that passed through an objective lens after reflection in a dichroic mirror. The SMS image during the 405-nm CW laser excitation in an Ar atmosphere is shown in Figure 2A. The laser excited both the radical precursor and Au_n, which allows us to perform the real-time observation of the newly formed Au_n. Initially, no fluorescence was observed, while successive laser excitation clearly caused an increase in individual fluorescent blinking species with a long off-time (Figures 2A and 2B).

The fluorescence spectra of the single Au_n are shown in Figure 2C. While the bulk fluorescence spectrum of Au_n was quite broad and indistinguishable, the single Au_n exhibited

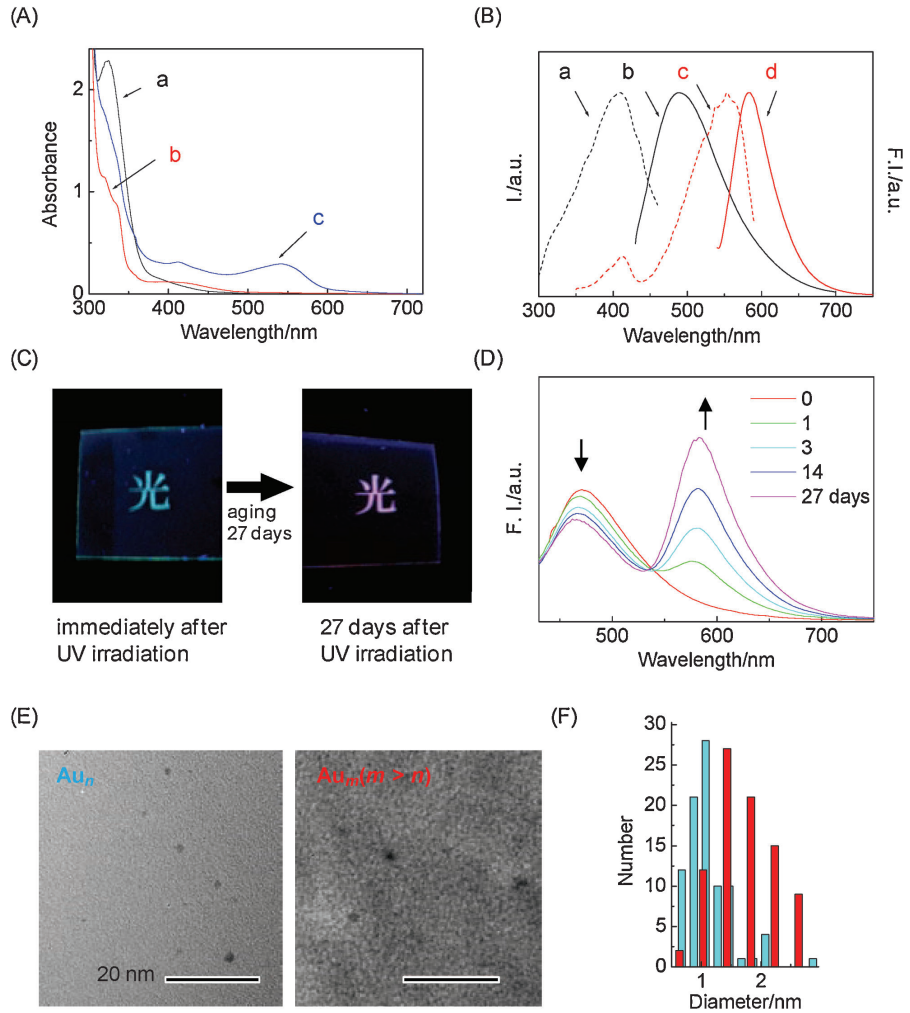

Figure 1. (A) The absorption spectra of the **PVAc** film before (black line, a) and after (red line, b) UV irradiation. The absorption spectrum of the aged **PVAc** film for 14 days after the UV-irradiation is also shown (blue line, c). (B) The excitation and emission spectra of Au clusters. Black lines a and b are excitation and emission spectra of Au_n (**PVAc** film immediately after UV-irradiation), respectively. Red lines c and d are excitation and emission spectra of Au_m ($m > n$) (aged **PVAc** film for 14 days after UV-irradiation), respectively. (C) Photograph of the emission from Au clusters in the **PVAc** film under the excitation of UV light. The Chinese character "light" was patterned using a photomask. The color of fluorescence changed from blue to pink during the aging for 27 days. (D) Time-resolved fluorescence spectra of the **PVAc** film after the UV irradiation. The film was excited by 380 nm light. (E) The TEM image of Au_n and Au_m ($m > n$). (F) The size distribution of Au_n (blue bar) and Au_m ($m > n$) (red bar). Copyright 2009 American Chemical Society.

much narrower fluorescence spectra. By taking into account the spectral response of the detection system, and in particular, the effect of cutoff filters, we concluded that the bulk spectrum of **PVAc** was composed of two main fluorescence spectra with peaks at 2.2 or >2.4 eV. Since the stability of Au_n, as well as its emission energy, depended on the n due to the closing of the electronic shell and the structure of the cluster, the histogram of the fluorescence maxima indicated that the distribution of the generated clusters was biased toward a favorable number of atoms (Figure 2D). Dickson et al. revealed that the relation between emission energy and atom number of Au clusters encapsulated by poly(amidoamine) dendrimers (PAMAM).[8,63] The emission energy of PAMAM-encapsulated Au clusters can be expressed by the jellium model (emission energy = $E_{Fermi}/n^{1/3}$, where E_{Fermi} is the Fermi energy of bulk Au.). According to the jellium model, several Au_n (n = 9–20) would exhibit emissions in the region from 2.1 to 2.6 eV. Au_{17} and $Au_{n<12}$ may correspond to the clusters emitting at 2.2 and >2.4 eV, respectively. No time-dependent spectral change in single Au_n was observed during the duration of the experiment, indicating that these clusters were very stable, and would experience no further growth and/or decomposition (ca. 5 min).

The fluorescence spectra of single Au_m ($m > n$) revealed that the bulk spectrum of Au_m ($m > n$) was mainly composed of the two spectra peaks at 1.97 and 2.04 eV, which may correspond to Au_{21} and Au_{19}, respectively (Figure 3). Taking into account the evolution of the fluorescence spectrum, a domain of Au clusters containing Au_n (n, <12 or 17) was generated during irradiation with UV light, and the distribution then slowly shifted to the Au_m (m, 19 or 21). The slow shift in distribution from Au_n (n, <12 or 17) to Au_m (m, 19 or 21) suggests the existence of a thermally accessible potential energy barrier

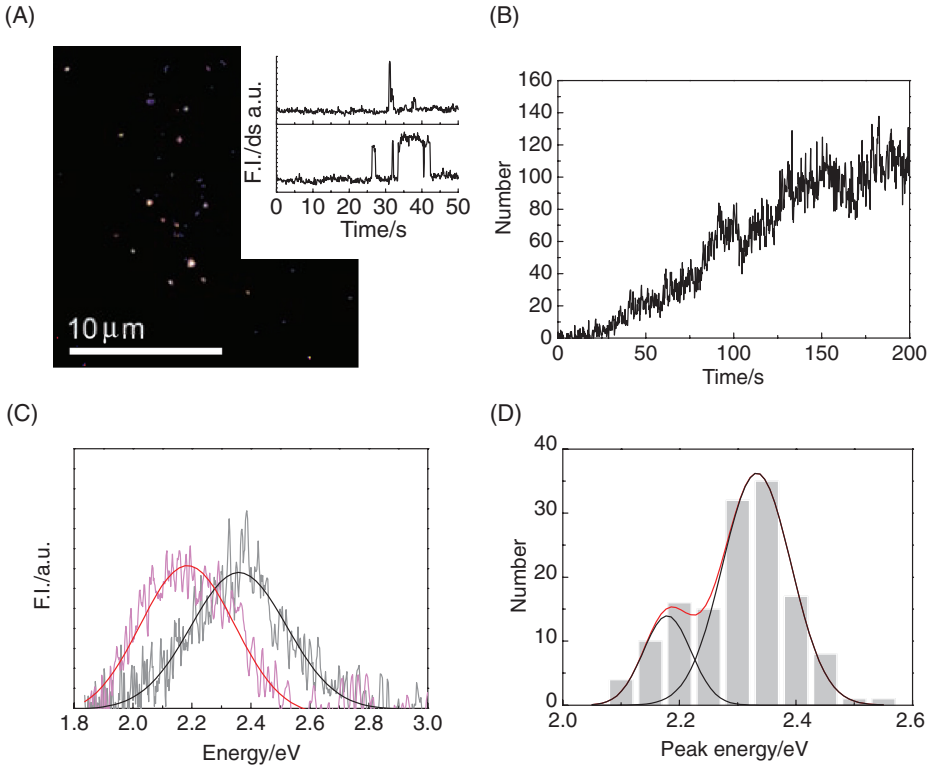

Figure 2. (A) SMS image under the excitation of a 405-nm laser for 60 s showing the photofabricated Au_n. Inset shows the typical fluorescence trajectories observed for single Au_n. (B) Time-dependent change in the number of fluorescent species. (C) Single-cluster fluorescence spectra. (D) The histogram of single-cluster emission peak. Emission maxima for typical single Au_n are ca. 2.2 and >2.4 eV. Copyright 2009 American Chemical Society.

between Au_n (n, <12 or 17) and Au_m (m, 19 or 21). The transition of the number of atoms assigned to the atom-by-atom growth process (i.e., the addition of a metal atom to a pre-formed Au cluster) seems to be more advantageous than the "cluster of clusters" process (i.e., successive additions of cluster units via sharing of atom) in the present system.[78] In polymer matrices, the diffusion of the clusters would be unfavorable compared with the diffusion of atoms.

1.2 Photochemical Reactivity of Au Clusters. Due to the molecule-like transitions involved, the photochemical reactivity of a quantized Au cluster is a subject of great interest. As regards molecular photochemistry, it is speculated that the photochemical reactivity of a molecule-like cluster depends on the structure (size) and the spin multiplicity of the excited state (i.e., singlet or triplet excited state). SMS analysis of Au clusters in polymer film allows us to investigate the photochemical reactivity of ligand-free Au clusters. Furthermore, since the fluorescence spectra of Au clusters are characterized by the number of atoms, SMS provides an opportunity to investigate the size-dependence of photochemical reactivity.

We investigated the photochemical reactivity of Au_n (n, <12 or 17) and Au_m (m, 19 or 21) to O_2.[75,76] O_2 is one of the most ubiquitous and fundamental quenchers of the excited states. The reaction with O_2 is also important from the viewpoint of applications, since it often determines the luminescence property of fluorescent labels.

SMS images of Au_n (n, <12 or 17) and Au_m (m, 19 or 21) embedded in thin PVAc film in an Ar- and O_2-saturated atmosphere are shown in Figure 4. The O_2 efficiently quenched the fluorescence of Au_n (n, <12 or 17). However, and remarkably, the opposite result was observed for Au_m (m, 19 or 21). The fluorescence intensity of Au_m (m, 19 or 21) increased with increasing O_2 concentration.

As shown in Figure 5, approximately 50% of the decreased Au_n (n, <12 or 17) was recovered by removing O_2. The fluorescence spectra and the histogram of the fluorescence maxima did not change significantly after this recovery. It was therefore concluded that there were two different quenching processes, that is, a reversible process and an irreversible process. The fluorescence quenching by O_2 was prohibited by capping the clusters with octadecanethiol, implying that the access of O_2 to the surface of the Au_n played a key role.

Various theoretical and experimental results have indicated that stable O_2-adsorption on negatively charged Au clusters occurs through (partial) charge transfer.[79–83] However, the reversibility of the observed reaction indicated that the fluorescence quenching did not proceed through strong interaction such as chemisorption, but rather, through a weak interaction. The binding energy of O_2 for Au_n with an odd n was dramatically smaller than that for Au clusters with an even n; therefore, the observed fluorescent species would be odd-numbered Au clusters.[79–83] Otherwise, the polymer might prohibit stable adsorption, because Au_n are partially stabilized through the interactions of the polymers.

We examined fluorescence quenching by using several electron acceptors (nitrobenzene, 1,4-dinitrobenzene, and nitro-

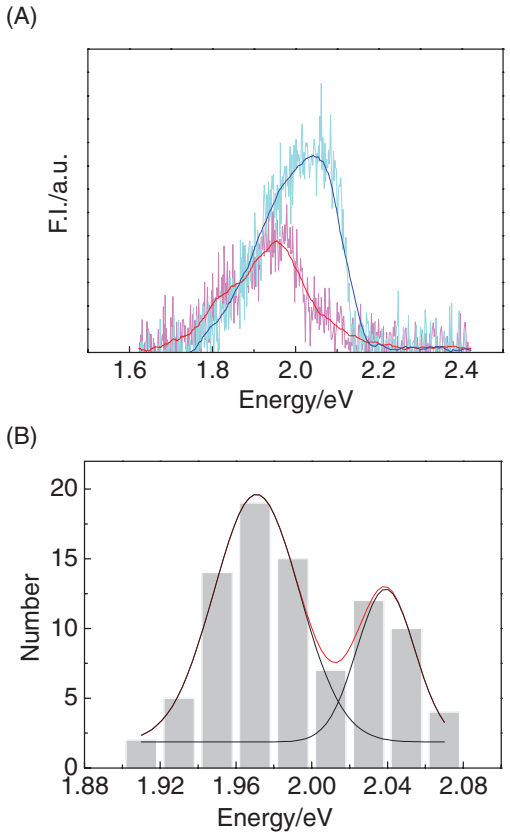

Figure 3. (A) Typical fluorescence spectra of single Au_m ($m > n$). (B) Histograms of single cluster emission peaks. Copyright 2009 American Chemical Society.

benzaldehyde with $E_{red} = -1.06$, -0.69, and -0.86 V vs. SCE, respectively).[84] Because the reduction potentials of these compounds are similar to that of O_2 ($E_{red} = -0.87$ V vs. SCE),[85] they quenched the fluorescence. It can therefore be speculated that photoinduced electron transfer was one of the reasons for the fluorescence quenching by O_2. The charge separation with and without recombination would be responsible for the reversible and irreversible processes, respectively (Scheme 3).

The increase in the number of atoms from n to m caused a dramatic change in the photochemical reactivity. In contrast to Au_n (n, <12 or 17), Au_m (m, 19 or 21) is inert to O_2. The driving force of photo-induced electron transfer is expressed by the oxidation/reduction potentials of donor/acceptor molecules and the energy gap between the ground and excited states (ΔE).[86,87] The ΔE of A_m (m, 19 or 21), which is smaller than that of Au_n (n, <12 or 17), could account for the difference in reactivity, because a larger ΔE is more favorable for the electron transfer. It is suggested that the electronic properties and O_2-affinity of Au clusters are also important factors.

The increase in the fluorescence intensity of Au_m in the presence of O_2 can be explained by the depopulation of the dark state by O_2. As in the previous SMS study, dark states were attributed to the triplet excited state and/or the reversible formation of a metastable less-fluorescent state.[88–91] The O_2-sensitive change of fluorescence intensity attribute to the intermolecular reaction between Au_m (m, 19 or 21) in the dark

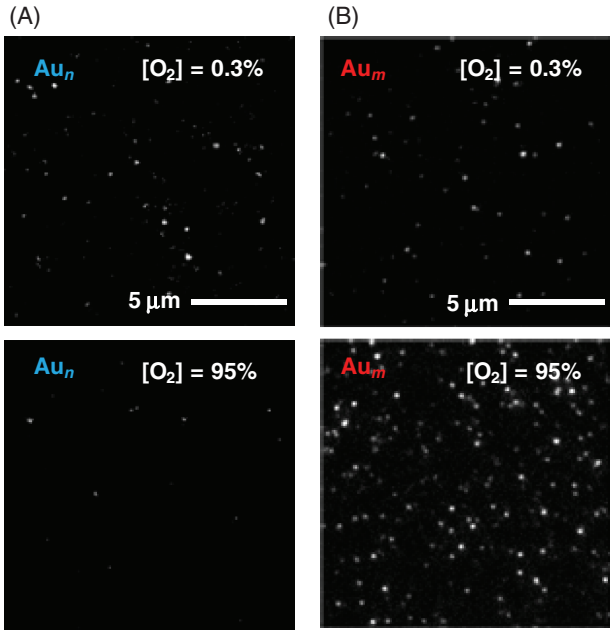

Figure 4. (A) SMS images of Au_n (n, <12 or 17) under the excitation of a 405-nm CW laser in an Ar- and O_2-saturated atmosphere. The emitters disappear in the presence of O_2. (B) SMS images of Au_m (m, 19 or 21) under the excitation of a 532-nm CW laser in Ar- and O_2-saturated atmospheres. The number of emitters dramatically increased in the presence of O_2. Copyright 2009 American Chemical Society.

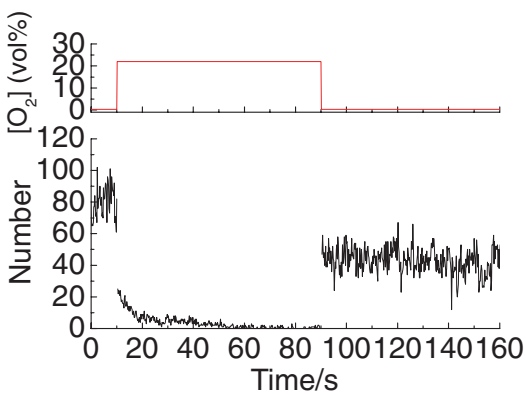

Figure 5. Dependence of the change in the number of fluorescent species on the O_2 concentration ($[O_2]$) in SMS image of Au_n (n, <12 or 17). The number of fluorescent species before O_2 exposure was around 80, and this number decreased to almost 0 after exposure to O_2 ($[O_2]$ = 22 vol %). Around 50 vol % of the decreased number of species was recovered by decreasing the $[O_2]$ to 0.3 vol %. Copyright 2009 American Chemical Society.

state and O_2. The dark state is the most likely triplet excited state, because O_2 is such an efficient triplet quencher.

To obtain evidence for the formation of Au_m (m, 19 or 21) in the triplet excited state, the phosphorescence of Au_m (m, 19 or 21) was measured. The emission of Au_m (m, 19 or 21) at 77 K in a 2-methyltetrahydrofuran (MTHF) matrix is shown in Figure 6. The emission peak was observed at 720 nm at 2 ms

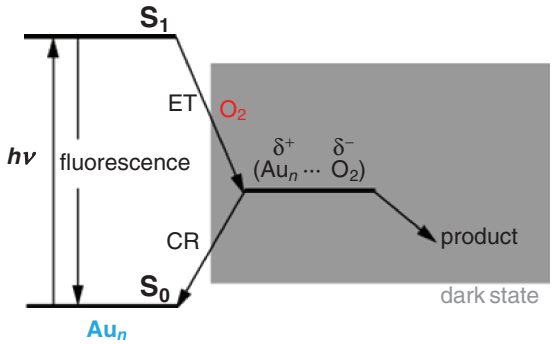

Scheme 3. Proposed energy-level diagram of Au_n (n, <12 or 17). The gray zone means the dark state. Au_n (n, <12 or 17) were excited by the 405-nm CW laser to form the singlet excited state (S_1). In the presence of O_2, Au_n (n, <12 or 17) in the S_1 state were quenched by O_2 via electron transfer (ET). A portion of Au_n (n, <12 or 17) recovers via charge recombination (CR). Copyright 2009 American Chemical Society.

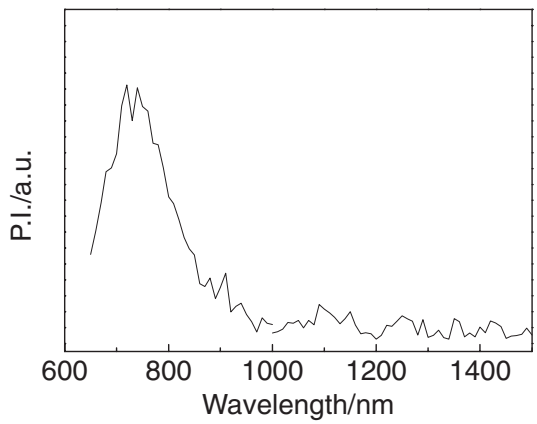

Figure 6. The phosphorescence spectrum of Au_m (m, 19 or 21) at 77K in the MTHF matrix observed 2 ms after the excitation with a pulsed 532-nm laser. Copyright 2009 American Chemical Society.

after pulsed 532-nm laser excitation. Since no emissions except for phosphorescence display such long-lived emissions, this emission can be defined as the phosphorescence of Au_m (m, 19 or 21).

We also successfully detected the near-IR luminescence spectrum of $^1O_2$ in PVAc film containing Au_m (m, 19 or 21).[76] The generation of $^1O_2$ indicates the formation of Au_m (m, 19 or 21) in the triplet excited state, because triplet energy transfer does not proceed from the singlet excited state. The generation of $^1O_2$ begins with the excitation of the Au_m (m, 19 or 21), following the formation of the singlet excited state, which is inert to O_2. The Au_m (m, 19 or 21) in the singlet excited state converts to the triplet excited state via intersystem crossing (ISC), and is quenched by energy transfer to O_2 in its triplet ground state (Scheme 4). The depopulation of Au_m in the triplet excited state (i.e., dark state) through the energy transfer to O_2 is the reason for the increase in fluorescence intensity.

The present study reveals the following: (1) Au_m (m, 19 or 21) has two different excited states, depending on the spin

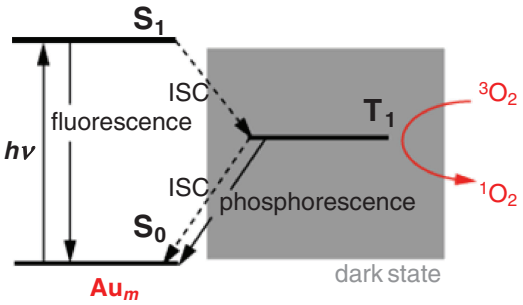

Scheme 4. Proposed energy-level diagram of Au_m. The gray zone means the dark state. Au_m (m, 19 or 21) were excited by the 532-nm CW laser to form the S_1. The Au_m (m, 19 or 21) in the S_1 is inert to the O_2. The formed S_1 state decays to the ground state (S_0) via radiative and non-radiative transitions: a portion is converted to the triplet excited state (T_1) through the intersystem crossing (ISC). The energy transfer to O_2 depopulates the triplet excited state (i.e., dark state) and increases the fluorescence intensity. Copyright 2009 American Chemical Society.

multiplicity (i.e., singlet or triplet excited state), and (2) these reactivities are dramatically different from each other. Unlike bulk metals, and similar to the case for organic molecules, the transition probability and the reactivity of Au clusters in the excited states are governed by spin multiplicity. It is necessary to emphasize another important result: the number of atoms in a cluster determines not only the electronic transition, but also the photochemical reactivity.

Although an Ag cluster is considered to be a powerful fluorescent-probe,[68–70] Au clusters are unfavorable, unfortunately, due to their blinking character and reactivity toward O_2. Our findings however, would eventually lead to further applications of Au clusters. A noble metal cluster with tunable spin multiplicity, photochemical properties, and reactivity is a promising material for various applications, such as photocatalysts, photodynamic therapy, photo-magnetic devices, and photoelectric conversion.

2. Photochemical Fabrication of Noble Metal NPs in a Polymer Matrix

Light can induce a desired photochemical reaction without damaging the surrounding environments. This is a powerful characteristic for the in situ fabrication of metal NPs in various mediums such as solutions, cells, polymer matrices, and glasses. The in situ synthesis of metal NPs in polymer matrices is also an important technique for the fabrication of NP/polymer composites. It is anticipated that these composites will have a broad range of applications in electronic, optical, and magnetic devices, as well as in improved plastics, because the composition of the NPs and polymers enhances such properties as conductivity, sustainability, and permeability with respect to neat polymer matrices.[92–97] In addition, it is noteworthy that the NPs in polymer film can be extracted by dissolving the polymer film into the solvent in the presence of stabilizer. We have developed a simple method of in situ photosensitization that uses photochemically generated radicals, and we applied it to the fabrication of Au NPs, Au/Cu core–shell-like NPs, and Ni^{2+}-adsorbed Au NPs in polymer matrices.[26,27,98]

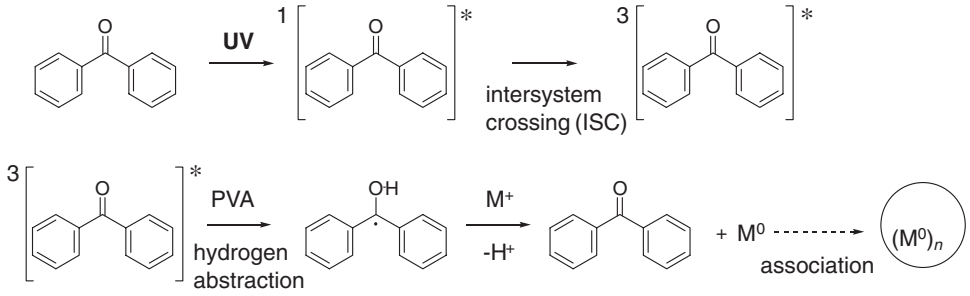

Scheme 5. Mechanism of photosensitized fabrication of metal NPs in a poly(vinyl alcohol) (PVA) film.

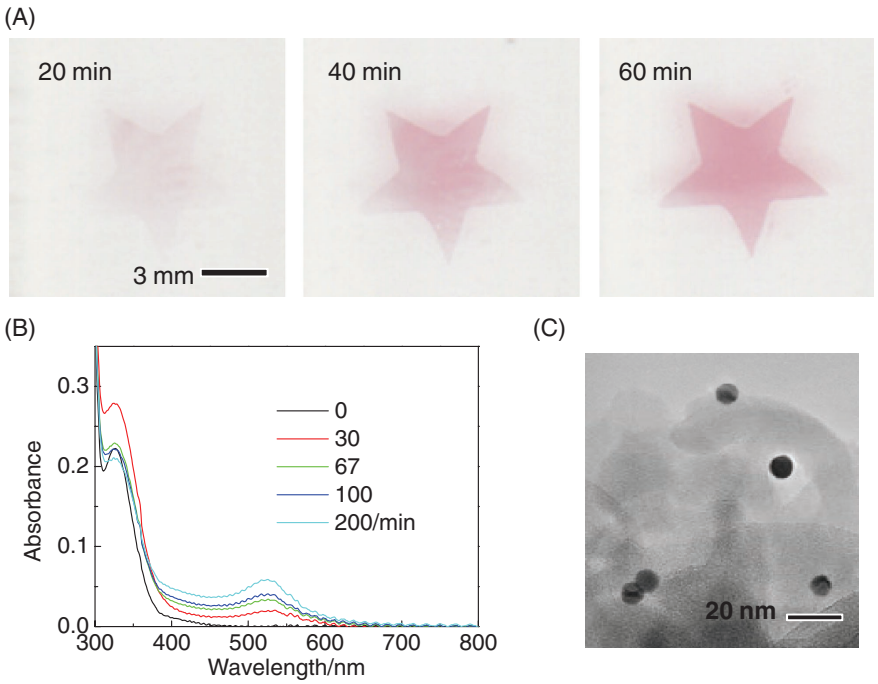

Figure 7. (A) Pictures of PVA film at 20, 40, and 60 min after the 355-nm pulse laser irradiation. (B) Time-resolved change of absorption spectra of PVA film containing BP and $H[AuCl_4]$ after the 355-nm laser irradiation. (C) TEM image of Au NPs fabricated in the PVA film via photochemical reaction. Copyright 2006 American Chemical Society.

2.1 Photochemical Fabrication of Au NPs in a Polymer Film. The mechanism of the photosensitized fabrication of metal NPs in a poly(vinyl alcohol) (PVA) film is shown in Scheme 5. A PVA film containing benzophenone (BP) and metal sources was prepared. BP and PVA work as a radical precursor and hydrogen donor, respectively. During irradiation by UV light, BP is excited and generates the triplet excited state ($BP(T_1)$). The $BP(T_1)$ abstracts hydrogen from the PVA to generate the ketyl radical ($BPH^{\bullet}$) and PVA radical. These radicals reduce the co-existing metal ions, leading to the formation of metal NPs.

Pictures of PVA film containing BP and $H[AuCl_4]$ after 355-nm pulsed laser irradiation (20 mJ pulse^{-1}, 50 shots) are shown in Figure 7A. After the pulsed laser irradiation, the color of the film gradually changed to magenta, due to the surface plasmon band of generated Au NPs (Figure 7B). The TEM image revealed that well-dispersed spherical Au NPs with diameters of 8–12 nm were generated by the pulsed laser irradiation (Figure 7C). The size of Au NPs generated in the PVA film was larger than that formed in the **PVAc** (see Section **1.1**). The polymer matrix, photosensitizer, and light source would be responsible for the difference of size.

We also investigated the photo-induced formation mechanism of Au NPs using laser flash photolysis. The transient absorption spectra of PVA film containing BP after the 355-nm laser irradiation are shown in Figure 8A. Upon excitation by the 355-nm laser (20 mJ pulse^{-1}, one shot), a strong absorption peak at 540 nm was observed. This absorption peak is assigned to BP in the triplet excited state, $BP(T_1)$. Five microseconds after the laser irradiation, the strong absorption disappeared and a broad absorption peak at around 550 nm was observed. Since the absorption peak at around 550 nm is assigned to $BPH^{\bullet}$, this spectral change indicates the formation of $BPH^{\bullet}$ through the hydrogen abstraction of $BP(T_1)$ from the PVA film. The lifetime of $BPH^{\bullet}$ significantly decreased with increasing concentration of $H[AuCl_4]$ in the PVA film, indicating the reduction of Au^{3+} by $BPH^{\bullet}$ (Figures 8B and 8C).

On the basis of these results, the entire process of photochemical fabrication of Au NPs in PVA film can be described as follows. During irradiation by UV light, the BP is excited to

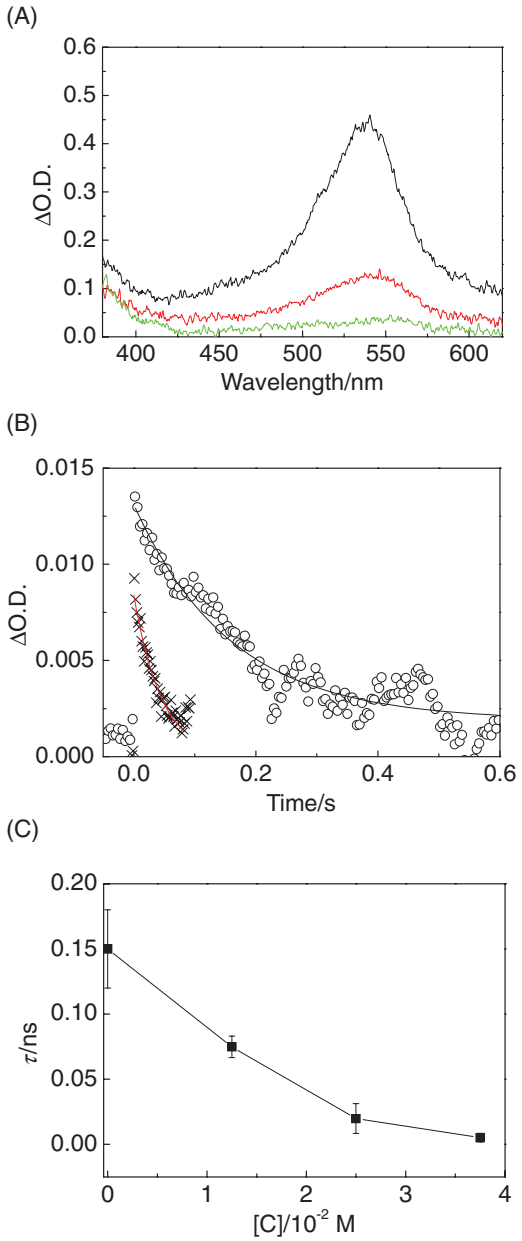

Figure 8. (A) Transient absorption spectra of PVA film containing BP and $H[AuCl_4]$ at 200 ns, 5 μs, and 500 μs (black, red, and green lines, respectively) after the 355-nm pulse laser irradiation. (B) Kinetic traces of PVA film containing BP (○) or BP and $H[AuCl_4]$ (×) at 540 nm after the 355-nm laser irradiation. (C) Life time (τ) of $BPH^{\bullet}$ vs. concentration of $H[AuCl_4]$ ([C]) in the PVA film. Copyright 2006 American Chemical Society.

the triplet excited state. The $BP(T_1)$ abstracts hydrogen from the PVA to generate the $BPH^{\bullet}$ and PVA radical (eq 1). These radicals reduce the Au^{3+} species to an Au^{2+} species, and this reaction triggers the formation of Au NPs (eqs 2 and 3). The formed Au^{2+} species disproportionate or are reduced by PVA, which leads to the formation of Au^{+} (eqs 4 and 5). The ketyl radical changes to a diphenyl methanol cation during the electron transfer. The diphenyl methanol cation deprotonates to regenerate the BP (Scheme 5).[99] The Au^{+} species disproportionate to form Au^0 (eq 6). The formed Au^0 are associated to form Au NPs. Interestingly, there was a long delay of several hours between the pulsed laser irradiation and the formation of Au NPs, implying a slow disproportionation of Au^{2+} and/or Au^{+} in the PVA film.

$$BP(T_1) + [-CH_2CH(OH)-]_n \rightarrow BPH^{\bullet} + [-CH_2\dot{C}(OH)-]_n \quad (1)$$

$$Au^{3+}Cl_4^- + BPH^{\bullet} \rightarrow Au^{2+}Cl_3^- + Cl + BP + H^+ \quad (2)$$

$$Au^{3+}Cl_4^- + [-CH_2\dot{C}(OH)-]_n \rightarrow Au^{2+}Cl_3^- + Cl + [-CH_2C{=}O-]_n + H^+ \quad (3)$$

$$Au^{2+}Cl_3^- + [-CH_2CH(OH)-]_n \rightarrow Au^{+}Cl_2^- + Cl + [-CH_2\dot{C}(OH)-]_n + H^+ \quad (4)$$

$$2Au^{2+}Cl_3^- \rightarrow Au^{+}Cl_2^- + Au^{3+}Cl_4^- \quad (5)$$

$$3Au^{+}Cl_2^- \leftrightarrow 2Au^0 + Au^{3+}Cl_4^- + 2Cl^- \quad (6)$$

The formation of Au NPs was significantly accelerated by the doping of formic acid into the film. For the PVA film doped with formic acid, an obvious color change was observed only 5 min after the 355-nm laser (3 mJ pulse^{-1}, 50 shots, 10 Hz) irradiation (Figure 9A). The evolution rate of the plasmon band became 20 times faster due to the doping (Figure 9B). The size and shape of AuNPs generated in formic-acid-doped PVA film were similar to those in undoped substrate.

We propose that the following mechanisms may be responsible for the acceleration. When $BP(T_1)$ abstracts a hydrogen atom from PVA, the hydrogen atom of formic acid should be competitively abstracted; i.e., $HCOO^{\bullet}$ should be generated as well as $BPH^{\bullet}$. Because $HCOO^{\bullet}$ was deprotonated to form H^+ and $CO_2^{\bullet-}$, $CO_2^{\bullet-}$ with a high reducing power reduces $[AuCl_4]^-$ and enhances the formation of the intermediate Au species.[100–102] Although the PVA radical is also expected to have a reducing ability, it should have a low mobility and reducing power. The PVA radical cannot efficiently reduce $[AuCl_4]^-$, as compared with $CO_2^{\bullet-}$. The second proposed mechanism is that the small Au NP works as a microelectrode that collects electrons from the formic acid.[103] No Au NP formation was observed without BP and laser irradiation, even in the presence of formic acid. Thus, it is suggested that the small Au NP was formed due to the reduction by $BPH^{\bullet}$ during the initial step. The small Au NP that was formed would work as a microelectrode and collect electrons from the formic acid. The Au ion reduction then occurs on the surface of the cathodically polarized Au particles, resulting in particle growth. Since the standard potential of the Au microelectrode was expected to decrease with increasing size of the nanoparticle, the formic acid may reduce the formed Au NPs, even though formic acid cannot reduce $[AuCl_4]^-$.[104–106] The third mechanism is the increase in the diffusion rate of Au ions in the swollen PVA film. According to the free volume theory, the diffusion constant of the solute was enhanced by swelling of the polymer films.[107–109] Since the disproportionation of Au ions was assumed to be one of the rate-determining steps of the Au NPs formation, the doping of formic acid to the PVA film may also accelerate the Au NPs formation in the PVA film.

2.2 Photochemical Fabrication of Bimetallic NPs in a Polymer Film. Bimetallic NPs are composed of two distinct metals. The synergy between two metals that constitute NPs

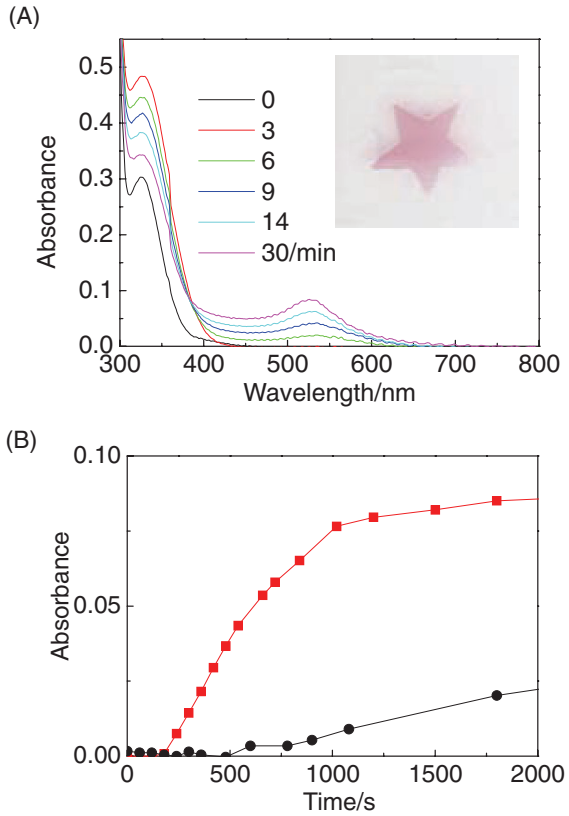

Figure 9. (A) Time-resolved absorption spectra of formic acid-doped PVA film (degree of doping 5.3 ± 1 wt %) containing BP and $H[AuCl_4]$ after the 355-nm pulse laser irradiation. Inset is a picture of formic acid-doped PVA (degree of doping 6 wt %) containing BP and $H[AuCl_4]$ at 5 min after the 355-nm pulsed laser irradiation. (B) Kinetic traces of the surface plasmon band of the PVA film containing BP and $H[AuCl_4]$ with two-different degrees of doping (black circles, 0.6 ± 0.3 wt %; red squares, 5.3 ± 1 wt %) by formic acid after the 355-nm pulsed laser irradiation. Copyright 2006 American Chemical Society.

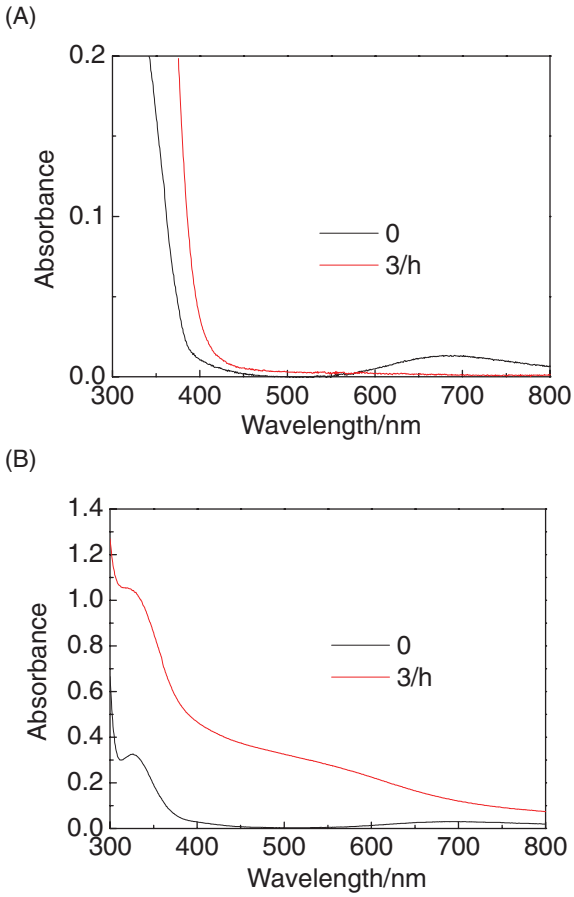

Figure 10. Absorption spectra of a PVA film before and after UV light irradiation. (A) Spectra corresponding to PVA film containing $Cu(CH_3COO)_2$ and BP, (B) PVA film containing $H[AuCl_4]$, $Cu(CH_3COO)_2$, and BP. Copyright 2007 Wiley-VCH Verlag GmbH & Co. KGaA.

often produces unique properties, including a better catalytic activity and selectivity than is produced by monometallic NPs.[7,15,24,110] We applied the BP/PVA system for the fabrication of bimetallic NPs.

In the case of PVA film containing BP and $Cu(CH_3COO)_2$, the surface plasmon band of Cu NPs was not observed after 365-nm UV-lamp (2.8 mW, Luv-16, AS one) irradiation, even though the broad absorption peak at around 680 nm, which can be ascribed to Cu^{2+}, disappeared (Figure 10A). This result can be explained as follows (Scheme 6). $BPH^{\bullet}$ and the PVA radicals can reduce Cu^{2+} to Cu^{+} (the reduction potential is 0.168 V vs. NHE).[111] However, they are unable to reduce Cu^{+} to Cu atom (the reduction potential is -2.7 V vs. NHE).[111,112]

The UV–vis absorption spectrum of a PVA film containing BP, $H[AuCl_4]$, and $Cu(CH_3COO)_2$, after UV irradiation, is shown in Figure 10B. The absorption spectrum, characterized by a broad absorbance, is similar to the surface plasmon band of Au/Cu core/shell bimetallic NPs fabricated in an aqueous solution.[113] Energy dispersive X-ray (EDX) analysis revealed that the NPs were Au/Cu core/shell-like structures.

The formation mechanism of Au/Cu bimetallic structures can be explained as follows (Scheme 6). $BPH^{\bullet}$ and PVA radicals reduce Au^{3+} to Au^{0}, but are not strong enough to reduce isolated Cu^{+} ions to Cu^{0}. They can, however, reduce Cu^{+} adsorbed on the Au core, since the reduction potential of metal ions increases upon adsorption on nuclei.[104,105] That is, Au cores were formed in the first stage, then the Cu^{+} reduced on the surface of the core led to the formation of bimetallic NPs. It is suggested that the core–shell-like structure of the NPs was formed by a phase separation. Although Cu and Au are completely soluble, the phase separation of the NPs may occur at room temperature, because the melting point of the NPs typically decreases as compared to that of the bulk.[114–116]

Interestingly, UV light (365 nm) irradiation of PVA film containing BP, $H[AuCl_4]$, and $Cu(CH_3COO)_2$ through a photomask formed a unique pattern. The color of the photoirradiated spot changed to dark brown due to the formation of Au/Cu bimetallic NPs (Figure 11, upper left photograph). Remarkably, pink and black double layers surrounding the dark brown pattern were observed.

TEM observations revealed that the NPs in the dark brown region had a spherical morphology of 1–8 nm in diameter (Figures 11A and 11E). The NPs formed in the pink layer

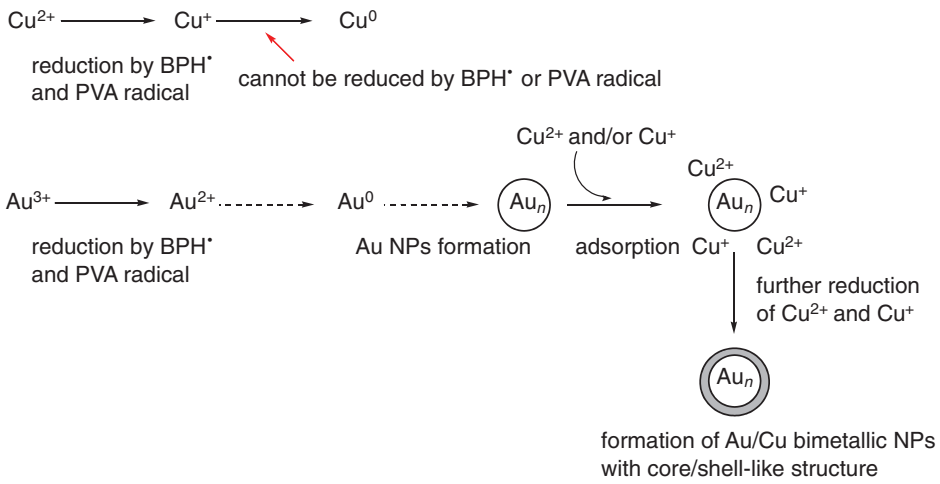

Scheme 6. The formation mechanism of Au/Cu bimetallic NPs.

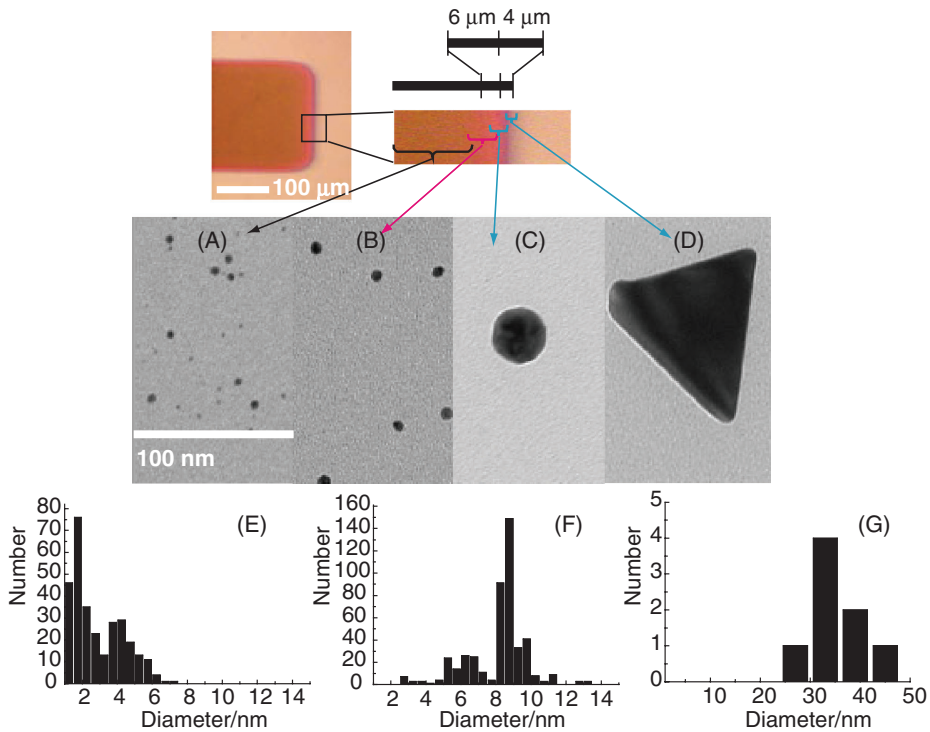

Figure 11. Photograph of a sample film and the TEM images at several positions on the pattern. The TEM images correspond to the microscope image on the upper part (A–D). Size distribution of NPs at position A in TEM image (E). Size distribution of NPs at position B in TEM image (F). Size distribution of NPs at position C in TEM image (G). Copyright 2007 Wiley-VCH Verlag GmbH & Co. KGaA.

surrounding the dark brown center were also spherical, and were two to three times larger than those in the dark brown region (Figures 11B and 11F). The NPs became larger (25–50 nm in diameter) close to the black layer (Figures 11C and 11G). Surprisingly, the NPs in the black layer exhibited a square morphology and were almost tetrahedral in shape (Figure 11D).

The different formation and growth mechanisms of NPs inside and outside the UV-light irradiation spot led to the differences in the size and shape in the PVA film. In the dark brown central region, the generated oxidative radicals reduce the metal complexes, and highly concentrated metal atoms and clusters are generated (Scheme 7A). Under such conditions, we can expect coalescence to be the main growth process of the NPs, due to the high concentration of metal atoms and clusters. In the case of growth via coalescence, the stabilizing effect of the PVA prevents the growth of the NPs beyond a certain nucleus size.[18] In the outer layers, a low concentration of metal atoms and clusters is continuously supplied from the light irradiation spot via diffusion. Under these conditions, small Au seeds are first formed. PVA is a mild reducing agent, and the Au ions adsorbed on the Au seeds were slowly reduced by the PVA, leading to the growth of larger NPs (Scheme 7B).[18,112,117]

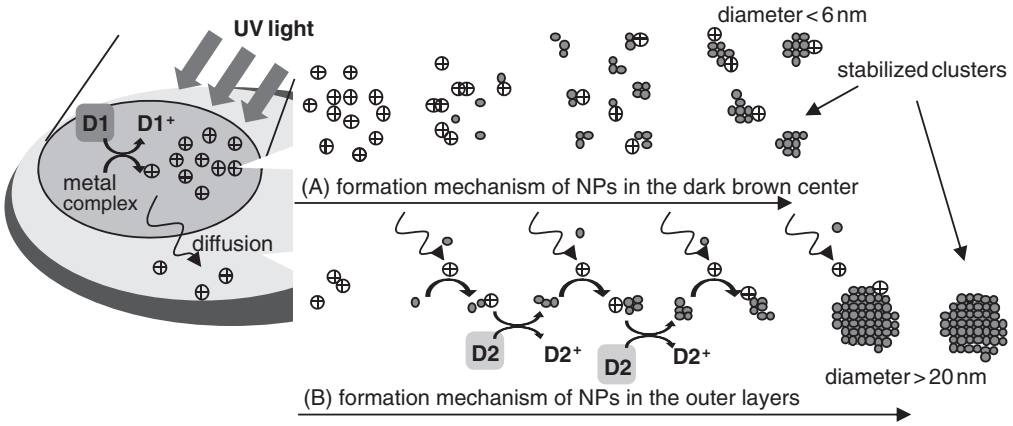

Scheme 7. Nucleation and growth mechanism of NPs in dark brown center (A) and outer layers (B). The plus symbol in the white circle denotes the $[AuCl_2]$ and Cu^+. The gray circle denotes the metal atom. D1 denotes the BPH$^\bullet$ and PVA radical. D2 denotes the PVA. The stabilizing effect of the PVA prevents coalescence beyond a certain limit of nuclearity in the dark brown center. However, the stepwise growths of the NPs by the reduction of metal ions on the surface of the NPs were not prevented and the NPs grew to a much larger size in the outer layers. Copyright 2007 Wiley-VCH Verlag GmbH & Co. KGaA.

In a subsequent investigation, we examined the co-reduction of Au and Ni ions in PVA film in a similar manner.[27] In this case, the Ni^{2+} or Ni^{2+} adsorbed on the surface of the Au NPs was not reduced by BPH$^\bullet$. Finally, Ni^{2+}-adsorbed Au NPs were formed in the PVA film. This indicates that the coexistence of metal ions is important for the formation of bimetallic NPs. By doping nitrilotriacetic acid (nta)-modified 5(6)-carboxyfluorescein (F-nta) into PVA film containing Ni^{2+}-adsorbed Au NPs, the F-nta formed an H-aggregate, due to the interaction between the nta and Ni^{2+} adsorbed on the Au NPs (Schemes 8 and 9).[118]

3. New Photosensitization Using Two Laser Beams with Different Wavelengths

The essence of photochemical synthesis of metal NPs is a photochemical reaction for the generation of M^0. The invention of a new photochemical process will lead to new avenues for the further development of methods of photochemical synthesis. We have proposed the photochemical reaction caused by stepwise excitation via two-photons of different wavelengths, as a new strategy in photochemical synthesis. In this section, we overview the mechanism of the photochemical production

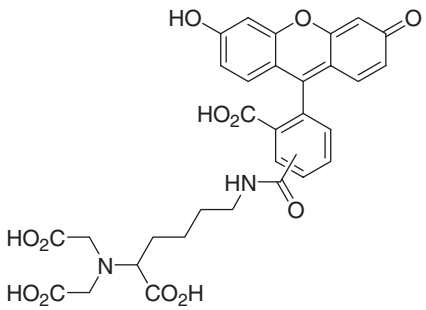

Scheme 8. Nitrilotriacetic acid (nta)-modified 5(6)-carboxyfluorescein (F-nta).

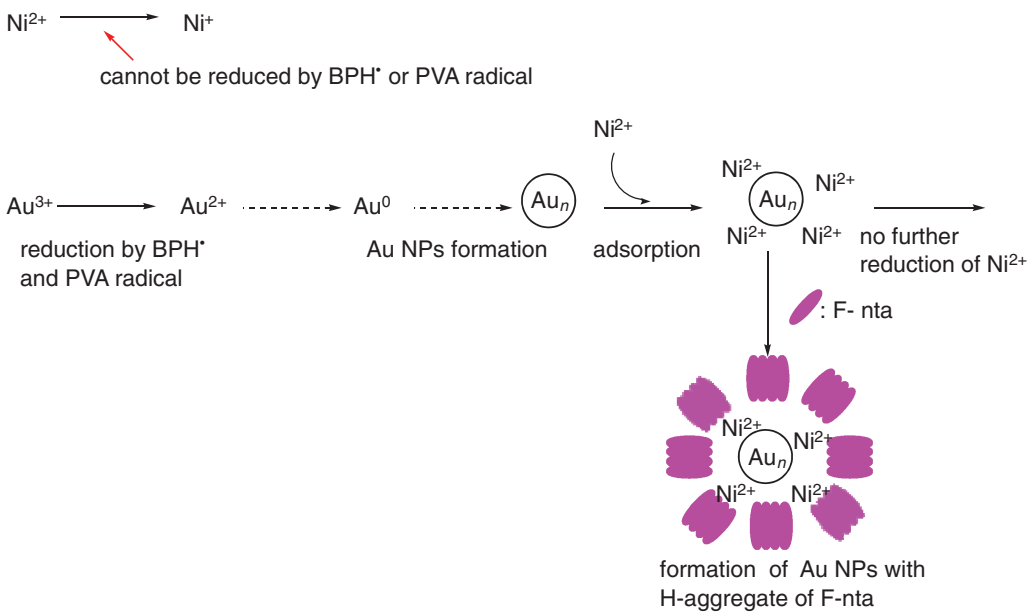

Scheme 9. Formation mechanism of Ni^{2+}-adsorbed Au NPs and attachment of F-nta on the surface.

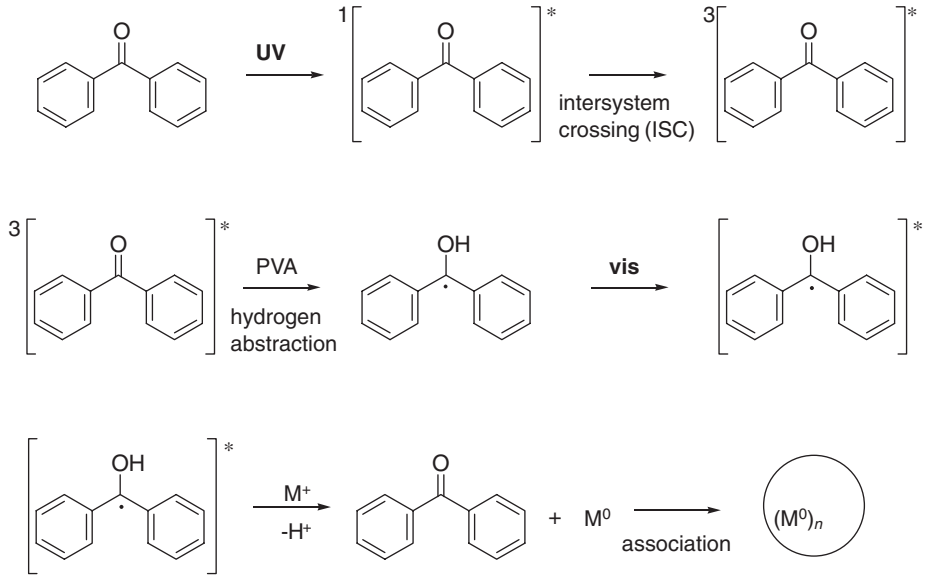

Scheme 10. The formation mechanism of metal NPs using $BPH^{\bullet}(D_1)$.

of M^0 using two light sources with different wavelengths and its application.

3.1 Photosensitization Using Excited Ketyl Radical. When radicals are excited, the excited state of the radicals is generated. Because an excited radical has various useful properties, such as emissivity and high reactivity, it has attracted great attention of scientists.[119–127] Our own interest has been attracted by the high reducing power of some excited radicals, which would reduce metal ions that cannot be reduced by ground-state radicals.[31,127] Reduction of metal ions with highly negative reduction potentials, such as Cu^+ as shown in Section **2.2**, expands the applicabilty of photosensitization.

To investigate the photosensitized fabrication of metal NPs using excited radicals, continuous wave lasers (UV, 363.8 nm and vis, 514.5 nm) were positioned so as to overlap on PVA film containing BP and $Cu(CH_3COO)_2$. CW lasers with a low density of photons were suitable for the precise control of the absorbed photon number. The UV laser excites BP to generate $BP(T_1)$. $BP(T_1)$ abstracts hydrogen from the PVA to form $BPH^{\bullet}$ and the PVA radical. In the overlapping area, the simultaneous irradiation of the vis laser excites $BPH^{\bullet}$ to generate $BPH^{\bullet}(D_1)$ (Scheme 10). Figure 12A shows the absorption spectra of a sample film before and after irradiation by the UV laser, and the simultaneous and stepwise irradiation of the UV and vis lasers. The evolution of the surface plasmon band of the Cu NPs was observed only after the simultaneous irradiation, indicating that $BPH^{\bullet}$ cannot reduce Cu^+ with a highly negative reduction potential, but that $BPH^{\bullet}(D_1)$ can reduce it (Scheme 11). The very strong reducing power of $BPH^{\bullet}(D_1)$ makes it possible to fabricate Cu NP in the PVA film, which cannot be done by the one-photon technique (Figure 12B). This strategy is expected to expand the applicability of the photosensitization in the synthesis of metal NPs.

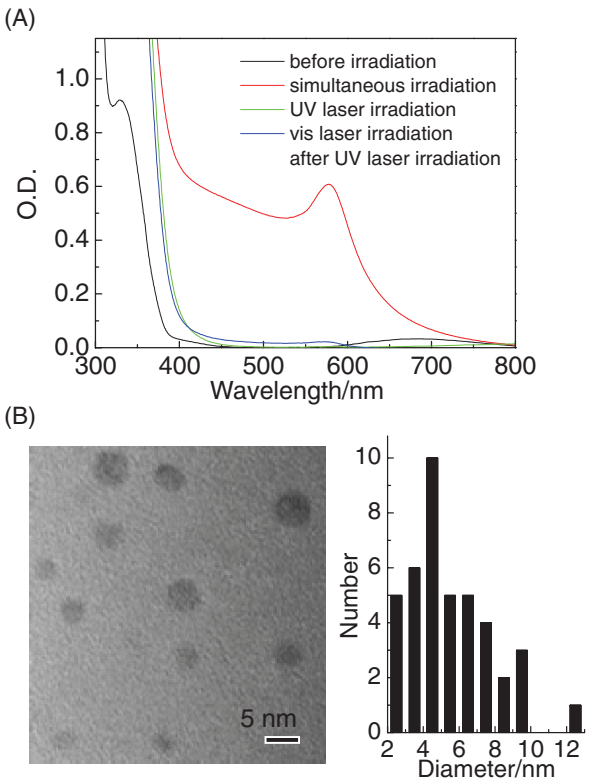

Figure 12. (A) UV–vis–near-IR absorption spectra of the PVA film containing BP and $Cu(CH_3COO)_2$ before and after laser irradiation (UV (363.8 nm) and vis laser (514.5 nm)). (B) The TEM images of the film after simultaneous irradiation for 30 min and the size distribution of Cu NP. The scale bar = 5 nm. Copyright 2008 American Chemical Society.

3.2 Photosensitization Using Carbazole in the Higher Excited State. As represented by Kasha's empirical rule, the majority of photochemical reactions proceed from the lowest excited state. The development of spectroscopy however has revealed that a variety of photochemical reactions proceed from higher excited states.[119,128–130] A considerable number of studies have been reported on a variety of reactions from higher excited states, such as bond cleavage, energy transfer, and electron transfer.

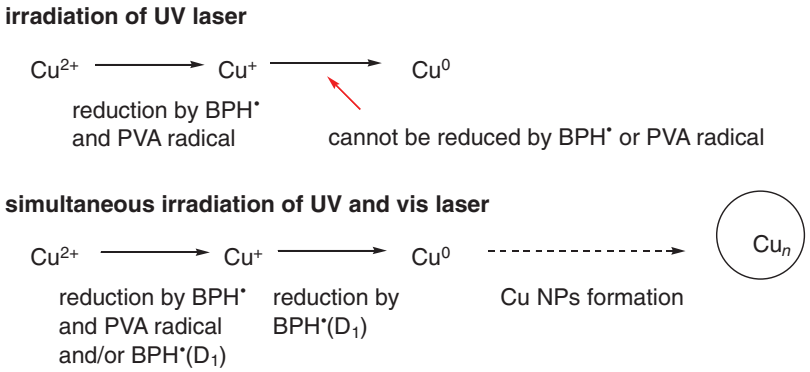

Scheme 11. The formation mechanism of Cu NPs using the $BPH^{\bullet}(D_1)$.

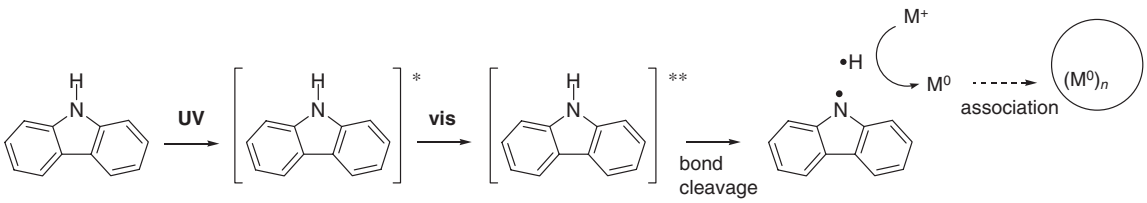

Scheme 12. The formation mechanism of metal NP using the bond dissociation of Cz in the higher excited state.

We introduced the concept of "bond cleavage from a higher excited state" to the photosensitized fabrication of metal NPs.[30] For example, the N–H bond dissociation of carbazole (Cz) does not occur from the lowest excited state, while it cleaves from the higher excited state and generates a carbazyl radical and a hydrogen atom (Scheme 12).[131] A hydrogen atom is a strong reducing agent, so it reduces the coexisting metal ions to generate metal NPs. The higher excited (S_n or T_n, $n > 1$) state can be achieved by the stepwise excitation of the precursor molecules.

A poly(methyl methacrylate) (PMMA) film containing Cz and $H[AuCl_4]$ was prepared. The UV–vis–near-IR absorption spectra of polymer films with a thickness of approximately 200–300 μm after single-laser, and after simultaneous two-color two-laser irradiation, are shown in Figure 13. A strong surface plasmon band of Au NP peaks at 536 nm was observed after simultaneous irradiation by two-color two-laser (UV and vis laser). In contrast, only a weak broad band from 400 to 600 nm was observed after single-laser irradiation. The surface plasmon band was not observed when the irradiation by the two lasers took place separately.

These results indicate that the hydrogen atom generated by the stepwise excitation of Cz reduce the $H[AuCl_4]$ to generate Au NPs. The simultaneous irradiation by two lasers with different wavelengths converts carbazole into a powerful photosensitizer. The photochemical fabrication of metal NPs completed by the two-color two-laser excitation can be utilized to the 3-D writing of metal NPs in the transparent matrices (see Section **4**).

3.3 Recyclable Photosensitization. The majority of organic photosensitizers for NPs synthesis are disposable and consumed during photochemical reactions. Due to this drawback, the amount of photosensitizer that is required is usually much larger than the amount of the metal source. For this reason, photosensitized fabrication of metal NPs is inadequate for circumstances that limit the amount of sensitizer, such as sensitizer-insoluble matrices and interfaces. The reaction cycle however offers a solution that can achieve efficient chemical reactions from limited reagents and energies. To overcome the

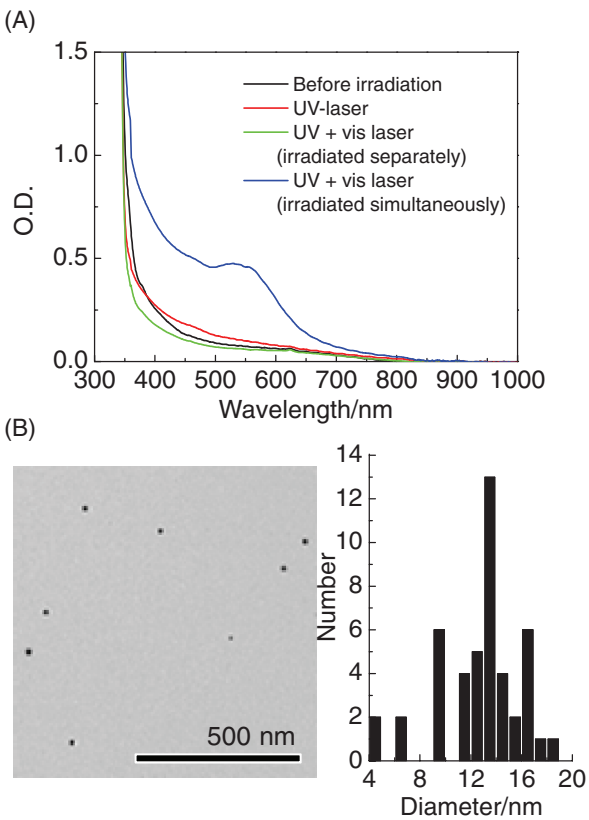

Figure 13. (A) UV–vis–near-IR absorption spectra of PMMA film containing Cz and $H[AuCl_4]$ before and after irradiation (2 h). (B) The TEM images of the film after the simultaneous irradiation for 2 h and the size distribution of Au NP.

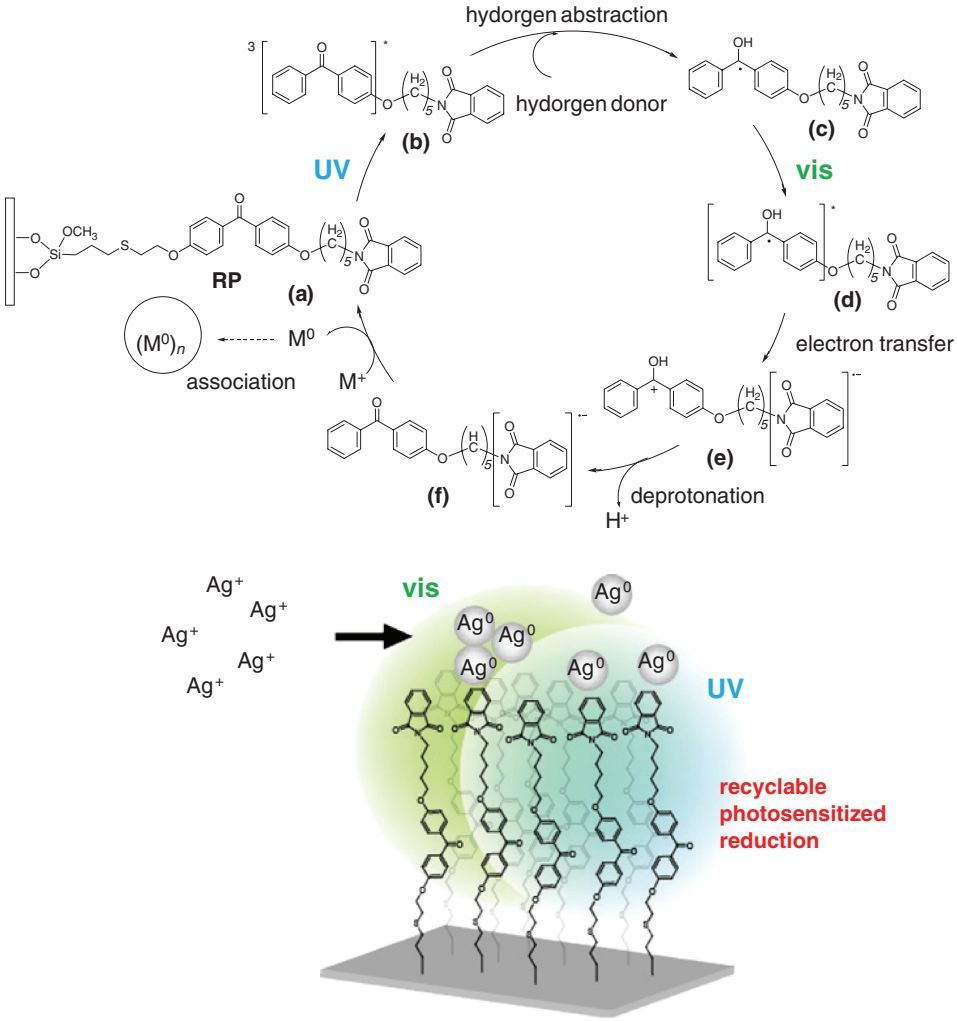

Scheme 13. Mechanism of recyclable photosensitization (upper scheme). The illustration of fabrication of Ag nanostructure at the solid–liquid interface using the recyclable photosensitization (lower scheme).

drawback of organic photosensitizers, we propose a recyclable photosensitization based on the concept of two-color two-photon excitation.[132,133]

The structure of the recyclable photosensitizer (RP) and the mechanism of cyclic reduction are shown in Scheme 13. In the first step, 4-methoxybenzophenone (MeOBP) chromophore of RP is excited by UV light to generate MeOBP(T_1) (state **b**). MeOBP(T_1) abstracts the hydrogen from the coexisting hydrogen donors to form the ketyl radical (MeOBPH$^{\bullet}$) (state **c**). Although MeOBPH$^{\bullet}$ cannot reduce *N*-methylphthalimide (MePI), the excited MeOBPH$^{\bullet}$ (MeOBPH$^{\bullet}$(D_1)) can reduce MePI.[120,122,126,132–134] The MeOBPH$^{\bullet}$(D_1) (state **d**) generated by a excitation by the vis laser reduces the MePI moiety to form a diphenylmethanol cation and an MePI radical anion (MePI$^{\bullet-}$) (state **e**). The diphenylmethanol cation quickly deprotonates to regenerate MeOBP (state **f**).[99,120,122,132–134] In the presence of an appropriate electron acceptor, the formed MePI$^{\bullet-}$ reduces the acceptors to regenerate the initial state **a**. As a result, the circular reaction is completed. The proposed cyclic reaction produces one reducing reagent (radical anion) and one proton from two photons (UV and vis light) and a hydrogen donor.

We attempted to apply this two-color two-photon induced recyclable photosensitization system to the fabrication of Ag nanostructures at the solid–liquid interface. The growth of crystals at the solid–liquid interface is an interesting process that helps us to understand the effect of external environmental factors (especially, the types of interfaces) on nanostructures. Furthermore, the structure and crystallographic orientation of inorganic crystals on a self-assembled monolayer has been reported to reflect the interaction between crystal phases and an organic monolayer.[135–137]

A RP-coordinated Si wafer was set in an aqueous 2-propanol solution of $AgNO_3$, then subjected to simultaneous irradiation by UV and vis light. 2-Propanol works as a hydrogen donor in this recyclable photosensitization. After laser irradiation of sufficient duration, recyclable photosensitization successfully fabricated a unique nanostructure at the solid–liquid interfaces.

Interestingly, the morphology of the generated Ag nanostructures was dependent on the type of substrate used, and the solvent polarity (Figure 14). In a polar solution (dielectric constant: $\varepsilon = 68$), wire-like Ag nanostructures were formed. On the other hand, in a less polar solution ($\varepsilon = 32$), plate-like structures were formed. The control experiments implied that

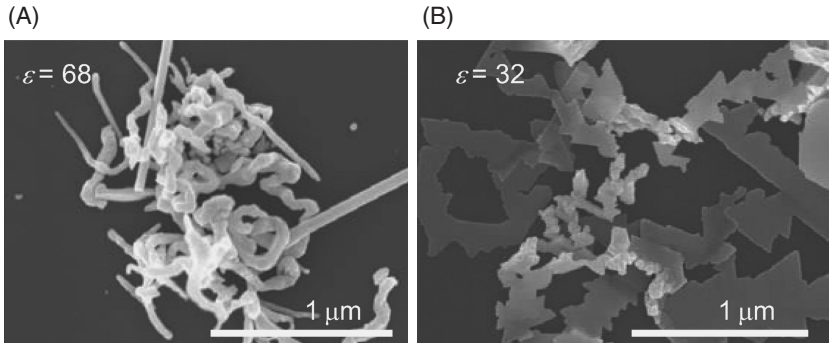

Figure 14. (A) SEM image of Ag nanostructure fabricated on RP-coordinated Si wafer during irradiation by two-color laser beams (2 h) in aqueous alcoholic solution ($\varepsilon_{mix} = 68$) of $AgNO_3$ (1 mM). (B) SEM image of Ag nanobelt fabricated on RP-coordinated Si wafer during irradiation by two-color laser beams (2 h) in aqueous alcoholic solution ($\varepsilon_{mix} = 32$) of $AgNO_3$ (1 mM). Copyright 2010 The Royal Society of Chemistry.

the formation of Ag nanowires in a polar solvent is assisted by the interaction between the Ag crystal phase and the surface of the substrate. On the other hand, light-induced shape variation and crystal growth caused by the Ostwald ripening process become pronounced in the less polar solvent, leading to the formation of Ag nanotriangles, which ultimately evolved into nanoplates.

In this photochemical approach, various solvents and surface-modified substrates can be applied. A better understanding of the factors that determine the morphology of nanostructures at the solid–liquid interface would enable us to develop better means of controlling the morphology of nanostructures.

4. Three-Dimensional Processing

The 3-D patterning and/or writing of materials is critical for several emerging technologies, including dense 3-D wiring for microelectronics, photonic crystals, metamaterials, optical memories, and microelectromechanical systems (MEMS).[41,138–140] The methodological exploration of the 3-D photochemical fabrication of metal NPs or continuous metal structure has been an area of unrelenting research. In this section, we describe the 3-D fabrication of metal NPs using photochemical methods.

Based on photosensitization using excited radicals or molecules in a higher excited state (see Section **3.1** and **3.2**), we have proposed a new approach to a 3-D writing technique that uses two or more laser beams of different wavelengths, i.e., multicolor laser processing (MCLP). MCLP is an alternative strategy for direct 3-D laser processing in which a multicolor-laser-induced reactive species such as excited radicals and molecules in higher excited states can be selectively generated in the area where the laser beams overlap. Because multicolor-laser-induced reactions, which proceed by stepwise multiphoton absorption, can be achieved by low-density photons, MCLP allows the internal processing of a laser ablative material without surface damage. Other advantage of multi-laser beams is the variability of the processable area in one session, due to the fact that it is adjustable (the area is equivalent to the area where the laser beams overlap).

We reported the 3-D fabrication of Cu NPs in a PVA matrix using the MCLP.[31] The strategy for the 3-D writing of Cu NP is shown in Figure 15. A UV laser (363.8 nm) and vis laser

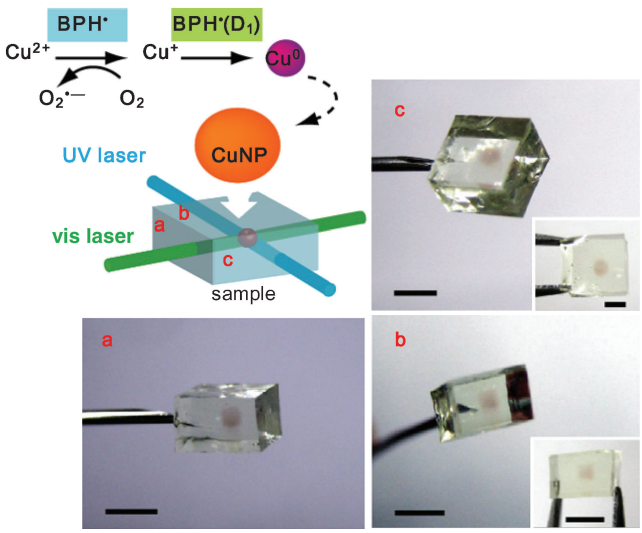

Figure 15. Photographs of 3-D Cu NP fabricated in a PVA block. Two lasers (UV laser (363.8 nm) and vis laser (514.5 nm)) were set perpendicular to each other to form the cross-point in the PVA film. The letters in the cartoon of the film correspond to the direction of the photograph. The scale bar = 3 mm. Copyright 2008 American Chemical Society.

(514.5 nm) were positioned to form a cross-point in PVA block containing BP and Cu^{2+}. A UV laser excited the BP in the PVA to generate $BPH^{\bullet}$ and the PVA radical. At the cross-point, the simultaneous irradiation by the vis laser excites $BPH^{\bullet}$ to generate $BPH^{\bullet}(D_1)$. Since only $BPH^{\bullet}(D_1)$ completes the reduction of Cu^{+} to Cu atom (Cu^0), Cu NP can be fabricated only at the cross-point of the two laser beams (See also Section **3.1**). By following this procedure, Cu NPs were three-dimensionally fabricated in the spherical area with diameters of around 1 mm in the PVA block, without any surface damage to the polymer matrix (Figure 15).

In related work, we demonstrated the 3-D fabrication of an array of Au NPs in the PVAc and PMMA matrix. In this case, carbazole was utilized as the precursor of the reductive intermediate. Although the N–H bond dissociation of carbazole did not occur from the lowest excited state, it is cleavable from the higher excited state. The N–H bond cleavage

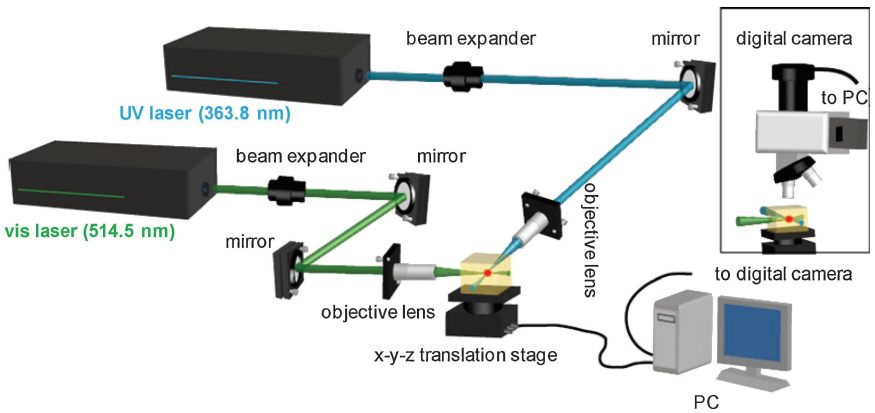

Scheme 14. The setup of MCLP. Copyright 2008 Wiley-VCH Verlag GmbH & Co. KGaA.

generates the highly reductive hydrogen atom, which reduces the coexisting Au^{3+} to Au^0.

The MCLP setup developed for this research is shown in Scheme 14. The two-color two-laser irradiation was carried out using an Ar-ion laser operating at 363.8 nm as the UV laser, and an Ar-ion laser operating at 514.5 nm as the vis laser. The laser beams were incident on the stage through a beam expander and were tightly focused on the sample by using objective lenses. The two laser beams were crossed using a pinhole (5 μm in diameter) and then adjusted by observing them under a microscope. The samples were mounted onto a computer-controlled *x*–*y*–*z* translation stage. By moving the translation stage, a 3-D Au NP array could be fabricated in the polymer matrices. The 3-D Au NP array in the polymer matrices was observed using a custom-made optical microscope equipped with a digital camera.

When the UV and vis laser were positioned to form a cross-point in the polymer matrix (PMMA and PVAc) containing $H[AuCl_4]$ and Cz, the Cz at the cross-point was sequentially excited by the UV and vis lasers to generate a higher excited state. The bond cleavage of Cz in the higher excited state formed a hydrogen atom, which reduced the coexisting $H[AuCl_4]$ to generate Au NPs. (See also Section **3.2**). As a result, Au NPs can be generated at the cross-point (Figure 16). Moving the cross-point using the computer-controlled stage allows the 3-D writing of the Au NP array in the polymer matrices. We fabricated a 3-D Chinese character "light" and a 3-D mesh design of the Au NP array with a line width of a few micrometers (Figures 16B and 16C).

When the two laser beams were crossed in the polymer matrices and the intensity (I_{vis}) of the vis laser was increased, we discovered that three kinds of photo-induced phenomena take place, depending on the I_{vis} (Figure 17). There are two threshold values for I_{vis}, I_{th1} and I_{th2} ($I_{th1} < I_{th2}$). When I_{vis} is relatively low, Au NPs formed at the cross-point of the laser beams (Figure 17A). Once the I_{vis} exceeded a threshold value ($I_{th1} < I_{vis}$), the Au NP formation area increased from the cross-point in the direction of the vis laser irradiation in a fluid-like manner (Figure 17B). We termed this phenomenon "laser-guided Au NP formation," which is different from the photochemical formation of Au NPs. Interestingly, the laser-guided Au NP formation area precisely traced the shape of the vis laser. For example, when the shape of the vis laser was

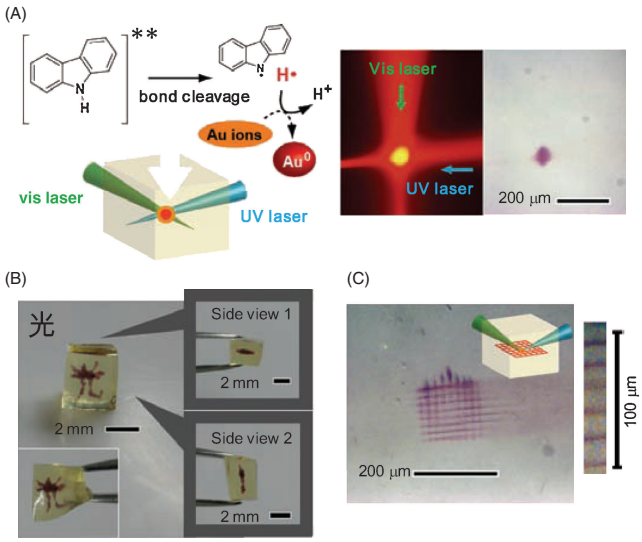

Figure 16. 3-D fabrication of Au NPs in the PVAc block containing Cz and $H[AuCl_4]$. (A) The illustration of mechanism of 3-D fabrication of Au NPs and microscope image of cross-point of two laser beams (left-hand-side image). (The image was obtained through an optical filter (Sigma Koki, SCF-50S-60R).) Optical microscope image of cross-point after simultaneous two-color two-laser irradiation (right-hand-side image). (B) 3-D Chinese character denoting "light" on the Au NP array written using MCLP. The image of the deformed flexible matrix held by tweezers is also shown. (C) Microscope image of 3-D mesh design of Au NP array and magnified image of lines. The line width is 4–5 μm. Copyright 2008 Wiley-VCH Verlag GmbH & Co. KGaA.

divided into three lines using a photomask, the Au NP formation area was also divided into three lines (microscopic image of b in Figure 17B).

At higher I_{vis} ($I_{th1} < I_{th2} < I_{vis}$), the formation of a microcavity surrounded by a thin Au NP/polymer composite layer was observed. The formed microcavity grew and shifted in the direction of the vis laser irradiation. Once the Au NP-formed area grew to the surface plane of the polymer block, gaseous decomposition products were ejected into the plume, and a microtunnel was formed (Figure 17C).

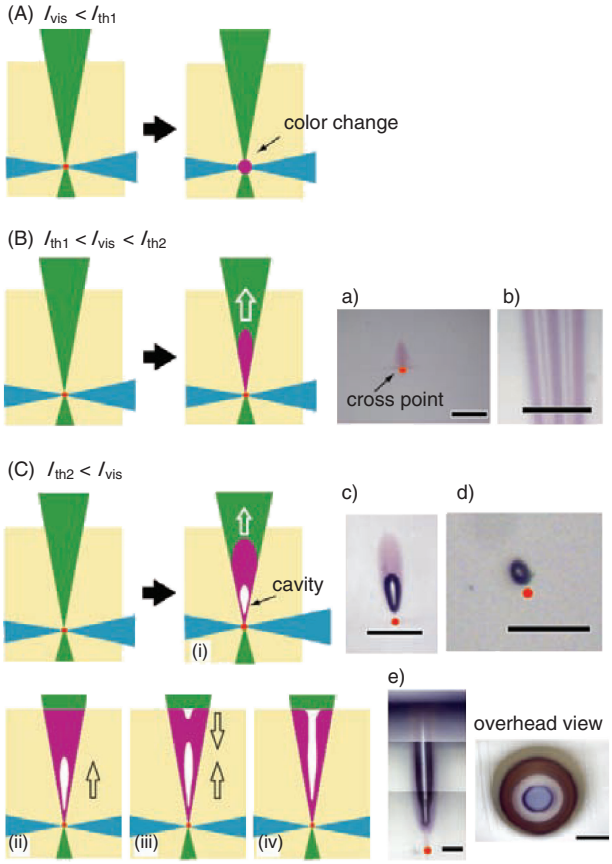

Figure 17. Photo-induced phenomena caused by two-color two-laser irradiation. The two laser beams are crossed at their focus. (A) Systematic illustration of photochemical formation of Au NPs. (B) Systematic illustration of laser-guided Au NP formation (left-hand-side image). a) Optical microscope images of Au NP array fabricated by laser-guided Au NP formation. The orange circle denotes the cross-point of laser beams. b) The laser-guided Au NP formation area traces the vis laser shape. Microscope images of Au NP formation area fabricated using vis laser divided into three-line is also shown. (C) Systematic illustration of space-selective cavity formation. (i) The microcavity is formed following the laser-guided Au NP formation. The microcavity grows gradually and moves toward the direction of the vis laser. (ii) Laser-guided Au NP formation area grows to the entrance plane toward the vis laser. (iii) Then, the material is ejected into the plume and a microtunnel is formed. (iv) Finally, the cavity and tunnel are connected. c) Optical microscope images of step (i). The orange circle denotes the cross-point of the laser beams. d) Spherical cavity with a diameter of 10 μm. e) Optical microscope images of step (iv). Scale bar = 200 μm. Copyright 2008 Wiley-VCH Verlag GmbH & Co. KGaA.

The relationship between the temperature of the Au NP (T_0) and the photo-induced events was examined (Figure 18). Under irradiation by a CW laser, T_0 is determined by the balance between I_{vis}, and the heat transfer from the NPs to the surrounding medium. According to the approach of Pustovalov,[141] the temperature of a spherical particle due to I_{vis} can be expressed by eq 7.

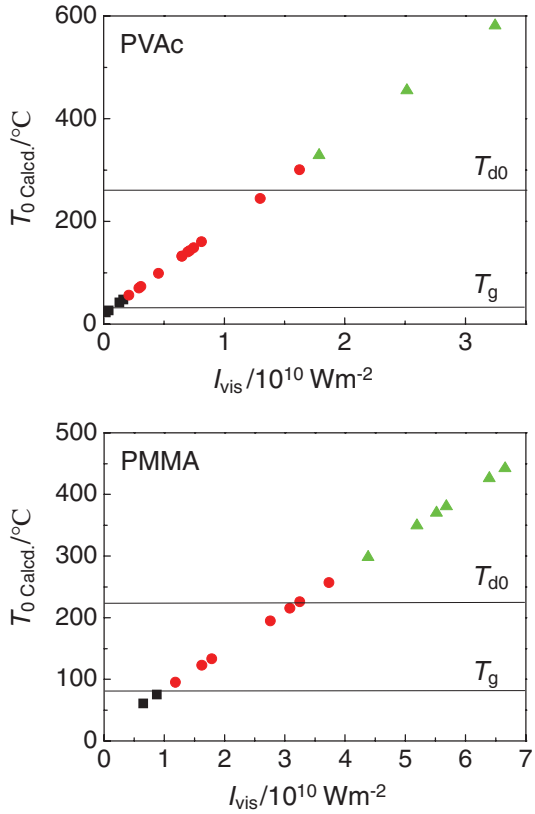

Figure 18. Relation between T_0 and occurrence of laser-guided Au NP and cavity formations in PVAc and PMMA. The symbols represent the observed phenomena, i.e., photochemical formation of Au NP array (black square), laser-guided Au NP formation (red circle) and cavity formation (green triangle).

$$T_0 = T_\infty + \frac{I_{vis} K_{abs} r_0}{4k_\infty} \quad (7)$$

where K_{abs} is the absorption efficiency factor for a particle with radius r_0, which can be calculated using the Mie scattering theory,[142] k_∞ is the thermal conductivity of the polymer, and T_∞ is the initial temperature (20 °C).

The temperatures at the starting point of the laser-guided Au NP and cavity formations were coincident with the glass transition temperature (T_g) and the temperature at which the total polymer decomposition began, respectively (T_{d0}).[143,144] These results indicate that these phenomena occurred due to the increase in the local temperature caused by the photothermal conversion of Au NPs.

From these considerations, the two laser-guided phenomena can be described as follows:

1. Au NPs are formed at the cross-point by the photochemical process ($I_{vis} < I_{th1}$).

2. The Au NPs formed in this manner convert the vis laser light into heat. Once the temperature exceeds T_g, the phase transition of a local polymer matrix proceeds from the cross-point in the direction of the vis laser. At the same time, the heat would cause the thermal fabrication of the Au NPs. These two concerted phenomena are termed laser-guided Au NP formation ($I_{th1} < I_{vis} < I_{th2}$).

3. When the temperature is sufficiently high to decompose the polymer, gaseous products are generated and pressure builds up inside the polymer matrix. Finally, the gas pressure becomes sufficiently large to eject the polymer matrix, and a cavity is formed ($I_{th2} < I_{vis}$).

The development of a novel 3-D processing technique for flexible materials is viewed as the key to several emerging advanced technologies such as dense flexible microelectronics, photonics, and MEMS.[145–148] The photo-induced phenomena we discovered offer the promise that the MCLP can be used for the fabrication of 3-D flexible microelectronics, MEMS, microfluidic channels, optical devices, and other applications.

Concluding Remarks and Future Prospects

In this account, we have attempted to describe the important and potential roles of photochemistry for the synthesis of metal NPs through a review of our recent studies. In this section, we summarize the results and discuss future prospects with regard to two important aspects of metal NPs synthesis: (i) investigation of formation mechanism and photochemical reactivity of metal NPs and (ii) synthesis of metal NPs.

(i) Investigation of Formation Mechanism and Photochemical Reactivity of Metal NPs. Photochemistry is effective for investigating the formation mechanisms of metal NPs. We employed SMS to observe the formation and growth mechanism of Au clusters. This approach successfully captured the individual clusters during the growth process and revealed the formation and growth process of Au clusters in the polymer film. This gave us important insight into the formation of metal NPs and the development of a method for the synthesis of metal nanoclusters with a precisely controlled number of atoms.

Due to its ability to facilitate the direct observation of growing metal NPs, microscopy offers great potential to reveal the formation mechanism of metal NPs. Recently, direct observation of growth process of metal NPs using the TEM achieves important results in this subject.[149,150] Optical or electron microscopy, combined with the photochemical fabrication of metal NPs, will become increasingly important as a means of investigating the formation and growth mechanisms of metal NPs.

Our investigation of individual ligand-free Au clusters provided important insights into photochemical reactivity. We discovered that Au clusters in the excited states display a variety of photochemical reactions that depend on the number of atoms and the spin multiplicity. In terms of photochemical reactivity, an Au cluster is similar to molecules, rather than to the bulk metal and larger NPs.

Although we acquired some degree of basic understanding of the photochemical reactivity of an Au cluster, many areas related to this research remain poorly understood. For example, the relationship between the structure of a metal cluster and reactivity is unclear. The development of new strategies for investigating bare clusters with a well-defined atom number and structure, is necessary for a better understanding of the photochemistry of metal clusters.

(ii) Synthesis of Metal NPs. The photochemical method is an important alternative in the synthesis of metal NPs. In situ photochemical synthesis is a useful method for the fabrication of metal NPs, as well as composite materials containing metal NPs. We have fabricated Au clusters, Au NPs, Au/Cu bimetallic NPs, and Ni^{2+} adsorbed Au NPs in polymer matrices using the in situ photochemical fabrication method. The in situ fabrication in a polymer matrix is a key to the formation of these nanostructures. The polymer matrix prevents the growth and/or aggregation of metal NPs, and promotes the formation of certain nanostructures.

The control of size and shape of metal NPs is important. It is believed that the size and shape of NPs in the polymer film are determined by environmental factors (i.e., interaction between metal atom and polymer and properties of polymer film) and formation process (i.e., formation mechanisms of metal atoms and density of irradiating light). For bimetallic NPs, the relation between redox potentials of metal sources and photosensitizer is an important factor determining the final structure. The systematic research for the formation and growth process of metal NPs in polymer film will help establishing better method to control the size, shape, and structure of NPs in the polymer film.

Advances in optical techniques will give researchers the opportunity to devise new strategies to obtain novel nanostructures and composite materials. The development of a novel photochemical reaction is directly linked to the progress of a photochemical method of synthesis of metal NPs. We developed a series of novel methods based on the stepwise excitation with different wavelengths of light. The multicolor excitation-induced photochemical reaction made possible the reduction of metal ions with a highly negative reduction potential, recyclable photosensitization, and the 3-D direct laser writing of metal NPs. These new strategies will expand the possible applications of the photochemical synthesis.

Finally, photochemistry plays an important role in various aspects of the synthesis of metal NPs. The characteristic properties of a photochemical reaction possess great potential to advance research into metal NPs. In future, the role of photochemistry will become increasingly important in the synthesis of metal NPs.

We are grateful to a number of colleagues, especially Dr. Takashi Tachikawa, Prof. Mamoru Fujitsuka, and co-workers for their experimental support, invaluable suggestions, and discussions. T.M. thanks to WCU (World Class University) program through the National Research Foundation of Korea funded by the Ministry of Education, Science and Technology (No. R31-10035) for the support. This work has been partly supported by a Grant-in-Aid for Scientific Research (Project Nos. 21710108, 22245022, and others) from the Ministry of Education, Culture, Sports, Science and Technology (MEXT) of Japanese Government.

References

1 R. W. Murray, *Chem. Rev.* **2008**, *108*, 2688.

2 S. Lal, S. E. Clare, N. J. Halas, *Acc. Chem. Res.* **2008**, *41*, 1842.

3 T. Laaksonen, V. Ruiz, P. Liljeroth, B. M. Quinn, *Chem. Soc. Rev.* **2008**, *37*, 1836.

4 P. K. Jain, X. Huang, I. H. El-Sayed, M. A. El-Sayed, *Acc. Chem. Res.* **2008**, *41*, 1578.

5 R. Wilson, *Chem. Soc. Rev.* **2008**, *37*, 2028.

6 M. E. Stewart, C. R. Anderton, L. B. Thompson, J. Maria, S. K. Gray, J. A. Rogers, R. G. Nuzzo, *Chem. Rev.* **2008**, *108*, 494.

7 R. Ferrando, J. Jellinek, R. L. Johnston, *Chem. Rev.* **2008**, *108*, 845.

8 J. Zheng, P. R. Nicovich, R. M. Dickson, *Annu. Rev. Phys. Chem.* **2007**, *58*, 409.

9 L. M. Liz-Marzán, *Langmuir* **2006**, *22*, 32.

10 M. A. El-Sayed, *Acc. Chem. Res.* **2004**, *37*, 326.

11 P. V. Kamat, *J. Phys. Chem. B* **2002**, *106*, 7729.

12 A. Henglein, *Chem. Rev.* **1989**, *89*, 1861.

13 J. H. Hodak, A. Henglein, G. V. Hartland, *J. Phys. Chem. B* **2000**, *104*, 9954.

14 Y. Xia, Y. Xiong, B. Lim, S. E. Skrabalak, *Angew. Chem., Int. Ed.* **2009**, *48*, 60.

15 T. Teranishi, M. Saruyama, M. Kanehara, *Chem. Lett.* **2009**, *38*, 194.

16 M. Sakamoto, M. Fujitsuka, T. Majima, *J. Photochem. Photobiol., A* **2009**, *10*, 33.

17 J. A. Dahl, B. L. S. Maddux, J. E. Hutchison, *Chem. Rev.* **2007**, *107*, 2228.

18 J. Belloni, *Catal. Today* **2006**, *113*, 141.

19 J. P. Wilcoxon, B. L. Abrams, *Chem. Soc. Rev.* **2006**, *35*, 1162.

20 I. Willner, R. Baron, B. Willner, *Adv. Mater.* **2006**, *18*, 1109.

21 C. J. Murphy, T. K. Sau, A. M. Gole, C. J. Orendorff, J. Gao, L. Gou, S. E. Hunyadi, T. Li, *J. Phys. Chem. B* **2005**, *109*, 13857.

22 B. L. Cushing, V. L. Kolesnichenko, C. J. O'Connor, *Chem. Rev.* **2004**, *104*, 3893.

23 M.-C. Daniel, D. Astruc, *Chem. Rev.* **2004**, *104*, 293.

24 N. Toshima, T. Yonezawa, *New J. Chem.* **1998**, *22*, 1179.

25 A. S. Korchev, M. J. Bozack, B. L. Slaten, G. Mills, *J. Am. Chem. Soc.* **2004**, *126*, 10.

26 M. Sakamoto, T. Tachikawa, M. Fujitsuka, T. Majima, *Adv. Funct. Mater.* **2007**, *17*, 857.

27 M. Sakamoto, T. Tachikawa, S. S. Kim, M. Fujitsuka, T. Majima, *ChemPhysChem* **2007**, *8*, 1701.

28 F. Stellacci, C. A. Bauer, T. Meyer-Friedrichsen, W. Wenseleers, V. Alain, S. M. Kuebler, S. J. K. Pond, Y. Zhang, S. R. Marder, J. W. Perry, *Adv. Mater.* **2002**, *14*, 194.

29 T. Deng, F. Arias, R. F. Ismagilov, P. J. A. Kenis, G. M. Whitesides, *Anal. Chem.* **2000**, *72*, 645.

30 M. Sakamoto, T. Tachikawa, M. Fujitsuka, T. Majima, *Adv. Mater.* **2008**, *20*, 3427.

31 M. Sakamoto, T. Tachikawa, M. Fujitsuka, T. Majima, *Chem. Mater.* **2008**, *20*, 2060.

32 S. Maruo, T. Saeki, *Opt. Express* **2008**, *16*, 1174.

33 T. Tanaka, A. Ishikawa, S. Kawata, *Appl. Phys. Lett.* **2006**, *88*, 081107.

34 Y. Shimotsuma, K. Hirao, P. G. Kazansky, J. Qiu, *Jpn. J. Appl. Phys.* **2005**, *44*, 4735.

35 J. Qiu, X. Jiang, C. Zhu, M. Shirai, J. Si, N. Jiang, K. Hirao, *Angew. Chem., Int. Ed.* **2004**, *43*, 2230.

36 P.-W. Wu, W. Cheng, I. B. Martini, B. Dunn, B. J. Schwartz, E. Yablonovitch, *Adv. Mater.* **2000**, *12*, 1438.

37 T. F. Scott, B. A. Kowalski, A. C. Sullivan, C. N. Bowman, R. R. McLeod, *Science* **2009**, *324*, 913.

38 Y.-Y. Cao, X.-Z. Dong, N. Takeyasu, T. Tanaka, Z.-S. Zhao, X.-M. Duan, S. Kawata, *Appl. Phys. A: Mater. Sci. Process.* **2009**, *96*, 453.

39 Y.-Y. Cao, N. Takeyasu, T. Tanaka, X.-M. Duan, S. Kawata, *Small* **2009**, *5*, 1144.

40 Y. Wang, W. Srituravanich, C. Sun, X. Zhang, *Nano Lett.* **2008**, *8*, 3041.

41 C. N. LaFratta, J. T. Fourkas, T. Baldacchini, R. A. Farrer, *Angew. Chem., Int. Ed.* **2007**, *46*, 6238.

42 S. Sun, P. Mendes, K. Critchley, S. Diegoli, M. Hanwell, S. D. Evans, G. J. Leggett, J. A. Preece, T. H. Richardson, *Nano Lett.* **2006**, *6*, 345.

43 A. Ishikawa, T. Tanaka, S. Kawata, *Appl. Phys. Lett.* **2006**, *89*, 113102.

44 K. Esumi, A. Suzuki, N. Aihara, K. Usui, K. Torigoe, *Langmuir* **1998**, *14*, 3157.

45 L. Berti, A. Alessandrini, P. Facci, *J. Am. Chem. Soc.* **2005**, *127*, 11216.

46 G. De Cremer, Y. Antoku, M. B. J. Roeffaers, M. Sliwa, J. Van Noyen, S. Smout, J. Hofkens, D. E. De Vos, B. F. Sels, T. Vosch, *Angew. Chem., Int. Ed.* **2008**, *47*, 2813.

47 K. Nishioka, Y. Niidome, S. Yamada, *Langmuir* **2007**, *23*, 10353.

48 O. R. Miranda, T. S. Ahmadi, *J. Phys. Chem. B* **2005**, *109*, 15724.

49 J. Pérez-Juste, I. Pastoriza-Santos, L. M. Liz-Marzán, P. Mulvaney, *Coord. Chem. Rev.* **2005**, *249*, 1870.

50 Y. Ohko, T. Tatsuma, T. Fujii, K. Naoi, C. Niwa, Y. Kubota, A. Fujishima, *Nat. Mater.* **2003**, *2*, 29.

51 Y. Niidome, K. Nishioka, H. Kawasaki, S. Yamada, *Chem. Commun.* **2003**, 2376.

52 F. Kim, J. H. Song, P. Yang, *J. Am. Chem. Soc.* **2002**, *124*, 14316.

53 J. Zhang, S. Li, J. Wu, G. C. Schatz, C. A. Mirkin, *Angew. Chem., Int. Ed.* **2009**, *48*, 7787.

54 J. E. Millstone, S. J. Hurst, G. S. Métraux, J. I. Cutler, C. A. Mirkin, *Small* **2009**, *5*, 646.

55 B. Pietrobon, V. Kitaev, *Chem. Mater.* **2008**, *20*, 5186.

56 I. Pastoriza-Santos, L. M. Liz-Marzán, *J. Mater. Chem.* **2008**, *18*, 1724.

57 A. Callegari, D. Tonti, M. Chergui, *Nano Lett.* **2003**, *3*, 1565.

58 R. Jin, Y. Cao, C. A. Mirkin, K. L. Kelly, G. C. Schatz, J. G. Zheng, *Science* **2001**, *294*, 1901.

59 To avoid any possible ambiguity, in this paper, we define NPs with a discrete density of states as "cluster". Goodson, Lee, et al. reported that the only Au NPs smaller than 2.2 nm shows the band gap.[60]

60 O. Varnavski, G. Ramakrishna, J. Kim, D. Lee, T. Goodson, *J. Am. Chem. Soc.* **2010**, *132*, 16.

61 W. A. de Heer, *Rev. Mod. Phys.* **1993**, *65*, 611.

62 R. B. Wyrwas, M. M. Alvarez, J. T. Khoury, R. C. Price, T. G. Schaaff, R. L. Whetten, *Eur. Phys. J. D* **2007**, *43*, 91.

63 J. Zheng, C. Zhang, R. M. Dickson, *Phys. Rev. Lett.* **2004**, *93*, 077402.

64 A. C. Templeton, W. P. Wuelfing, R. W. Murray, *Acc. Chem. Res.* **2000**, *33*, 27.

65 C. I. Richards, S. Choi, J.-C. Hsiang, Y. Antoku, T. Vosch, A. Bongiorno, Y.-L. Tzeng, R. M. Dickson, *J. Am. Chem. Soc.* **2008**, *130*, 5038.

66 M. Haruta, *Chem. Rec.* **2003**, *3*, 75.

67 S. Kanaoka, N. Yagi, Y. Fukuyama, S. Aoshima, H. Tsunoyama, T. Tsukuda, H. Sakurai, *J. Am. Chem. Soc.* **2007**, *129*, 12060.

68 T.-H. Lee, J. I. Gonzalez, J. Zheng, R. M. Dickson, *Acc.*

Chem. Res. **2005**, *38*, 534.
69 T. Vosch, Y. Antoku, J.-C. Hsiang, C. I. Richards, J. I. Gonzalez, R. M. Dickson, *Proc. Natl. Acad. Sci. U.S.A.* **2007**, *104*, 12616.
70 J. Yu, S. A. Patel, R. M. Dickson, *Angew. Chem., Int. Ed.* **2007**, *46*, 2028.
71 G. Ramakrishna, O. Varnavski, J. Kim, D. Lee, T. Goodson, *J. Am. Chem. Soc.* **2008**, *130*, 5032.
72 Z. Wu, C. Gayathri, R. R. Gil, R. Jin, *J. Am. Chem. Soc.* **2009**, *131*, 6535.
73 Z. Wu, R. Jin, *ACS Nano* **2009**, *3*, 2036.
74 C. Zander, J. Enderlein, R. A. Keller, *Single Molecule Detection in Solution*, WILEY-VCH, Verlag Berlin GmbH, Berlin, **2002**.
75 M. Sakamoto, T. Tachikawa, M. Fujitsuka, T. Majima, *J. Am. Chem. Soc.* **2009**, *131*, 6.
76 M. Sakamoto, T. Tachikawa, M. Fujitsuka, T. Majima, *Langmuir* **2009**, *25*, 13888.
77 T. Tachikawa, T. Majima, *Langmuir* **2009**, *25*, 7791.
78 B. K. Teo, H. Zhang, *Coord. Chem. Rev.* **1995**, *143*, 611.
79 B. E. Salisbury, W. T. Wallace, R. L. Whetten, *Chem. Phys.* **2000**, *262*, 131.
80 D. H. Wells, W. N. Delgass, K. T. Thomson, *J. Chem. Phys.* **2002**, *117*, 10597.
81 B. Yoon, H. Häkkinen, U. Landman, *J. Phys. Chem. A* **2003**, *107*, 4066.
82 D. Stolcic, M. Fischer, G. Ganteför, Y. D. Kim, Q. Sun, P. Jena, *J. Am. Chem. Soc.* **2003**, *125*, 2848.
83 B. Yoon, P. Koskinen, B. Huber, O. Kostko, B. von Issendorff, H. Häkkinen, M. Moseler, U. Landman, *ChemPhysChem* **2007**, *8*, 157.
84 M. Montalti, A. Credi, L. Prodi, M. T. Gandolfi, *Handbook of Photochemistr*y, 3rd. ed., CRC Press, Boca Raton, FL 33487–2742, **2006**.
85 D. T. Sawyer, G. Chiericato, C. T. Angelis, E. J. Nanni, T. Tsuchiya, *Anal. Chem.* **1982**, *54*, 1720.
86 R. A. Marcus, *Annu. Rev. Phys. Chem.* **1964**, *15*, 155.
87 G. J. Kavarnos, N. J. Turro, *Chem. Rev.* **1986**, *86*, 401.
88 W.-T. Yip, D. Hu, J. Yu, D. A. Vanden Bout, P. F. Barbara, *J. Phys. Chem. A* **1998**, *102*, 7564.
89 J. A. Veerman, M. F. Garcia-Parajo, L. Kuipers, N. F. van Hulst, *Phys. Rev. Lett.* **1999**, *83*, 2155.
90 D. S. English, A. Furube, P. F. Barbara, *Chem. Phys. Lett.* **2000**, *324*, 15.
91 S. J. Park, A.-J. Gesquiere, J. Yu, P. F. Barbara, *J. Am. Chem. Soc.* **2004**, *126*, 4116.
92 A. C. Balazs, T. Emrick, T. P. Russell, *Science* **2006**, *314*, 1107.
93 L. Nicolais, G. Carotenuto, *Metal–Polymer Nanocomposite*, John Wiley & Sons, Hoboken, NJ, **2005**.
94 R. A. Vaia, J. F. Maguire, *Chem. Mater.* **2007**, *19*, 2736.
95 G. V. Ramesh, S. Porel, T. P. Radhakrishnan, *Chem. Soc. Rev.* **2009**, *38*, 2646.
96 J. Shan, H. Tenhu, *Chem. Commun.* **2007**, 4580.
97 A. Haryono, W. H. Binder, *Small* **2006**, *2*, 600.
98 M. Sakamoto, T. Tachikawa, M. Fujitsuka, T. Majima, *Langmuir* **2006**, *22*, 6361; Erratum: M. Sakamoto, T. Tachikawa, M. Fujitsuka, T. Majima, *Langmuir* **2007**, *23*, 7886.
99 M. Bietti, O. Lanzalunga, *J. Org. Chem.* **2002**, *67*, 2632.
100 M. Mrowetz, W. Balcerski, A. J. Colussi, M. R. Hoffmann, *J. Phys. Chem. B* **2004**, *108*, 17269.
101 L. L. Perissinotti, M. A. Brusa, M. A. Grela, *Langmuir* **2001**, *17*, 8422.
102 N. R. de Tacconi, H. Wenren, D. McChesney, K. Rajeshwar, *Langmuir* **1998**, *14*, 2933.
103 A. L. Rogach, G. P. Shevchenko, Z. M. Afanas'eva, V. V. Sviridov, *J. Phys. Chem. B* **1997**, *101*, 8129.
104 A. Henglein, *J. Phys. Chem.* **1993**, *97*, 5457.
105 S. Mosseri, A. Henglein, E. Janata, *J. Phys. Chem.* **1989**, *93*, 6791.
106 K. Mallik, M. Mandal, N. Pradhan, T. Pal, *Nano Lett.* **2001**, *1*, 319.
107 H. Yasuda, C. E. Lamaze, L. D. Ikenberry, *Makromol. Chem.* **1968**, *118*, 19.
108 H. Yasuda, A. Peterlin, C. K. Colton, K. A. Smith, E. W. Merrill, *Makromol. Chem.* **1969**, *126*, 177.
109 H. Matsuyama, M. Teramoto, H. Urano, *J. Membr. Sci.* **1997**, *126*, 151.
110 L. Guczi, *Catal. Today* **2005**, *101*, 53.
111 A. S. Korchev, T. S. Shulyak, B. L. Slaten, W. F. Gale, G. Mills, *J. Phys. Chem. B* **2005**, *109*, 7733.
112 E. Gachard, H. Remita, J. Khatouri, B. Keita, L. Nadjo, J. Belloni, *New J. Chem.* **1998**, *22*, 1257.
113 A. K. Sra, R. E. Schaak, *J. Am. Chem. Soc.* **2004**, *126*, 6667.
114 K. Dick, T. Dhanasekaran, Z. Zhang, D. Meisel, *J. Am. Chem. Soc.* **2002**, *124*, 2312.
115 T. Shibata, B. A. Bunker, Z. Zhang, D. Meisel, C. F. Vardeman, II, J. D. Gezelter, *J. Am. Chem. Soc.* **2002**, *124*, 11989.
116 J. G. Lee, H. Mori, H. Yasuda, *Phys. Rev. B* **2002**, *66*, 012105.
117 L. Longenberger, G. Mills, *J. Phys. Chem.* **1995**, *99*, 475.
118 D. Tareste, F. Pincet, M. Brellier, C. Mioskowski, É. Perez, *J. Am. Chem. Soc.* **2005**, *127*, 3879.
119 J. C. Scaiano, L. J. Johnston, W. G. McGimpsey, D. Weir, *Acc. Chem. Res.* **1988**, *21*, 22.
120 M. Sakamoto, X. Cai, M. Fujitsuka, T. Majima, *J. Phys. Chem. A* **2005**, *109*, 6830.
121 M. Sakamoto, X. Cai, M. Fujitsuka, T. Majima, *J. Phys. Chem. A* **2006**, *110*, 9788.
122 M. Sakamoto, X. Cai, M. Fujitsuka, T. Majima, *J. Phys. Chem. A* **2006**, *110*, 11800.
123 M. Sakamoto, X. Cai, M. Hara, M. Fujitsuka, T. Majima, *J. Phys. Chem. A* **2005**, *109*, 2452.
124 M. Sakamoto, X. Cai, M. Hara, S. Tojo, M. Fujitsuka, T. Majima, *J. Am. Chem. Soc.* **2005**, *127*, 3702.
125 M. Sakamoto, X. Cai, M. Hara, S. Tojo, M. Fujitsuka, T. Majima, *J. Phys. Chem. A* **2004**, *108*, 8147.
126 M. Sakamoto, X. Cai, M. Fujitsuka, T. Majima, *Chem.—Eur. J.* **2006**, *12*, 1610.
127 M. Sakamoto, T. Tachikawa, M. Fujitsuka, T. Majima, *Chem. Phys. Lett.* **2006**, *420*, 90; Erratum: M. Sakamoto, T. Tachikawa, M. Fujitsuka, T. Majima, *Chem. Phys. Lett.* **2007**, *442*, 170.
128 M. Sakamoto, X. Cai, M. Hara, M. Fujitsuka, T. Majima, *J. Am. Chem. Soc.* **2004**, *126*, 9709.
129 M. Sakamoto, X. Cai, M. Hara, M. Fujitsuka, T. Majima, *J. Phys. Chem. A* **2005**, *109*, 4657.
130 M. Sakamoto, X. Cai, M. Hara, S. Tojo, M. Fujitsuka, T. Majima, *J. Phys. Chem. A* **2004**, *108*, 10941.
131 M. Martin, E. Breheret, F. Tfibel, B. Lacourbas, *J. Phys. Chem.* **1980**, *84*, 70.
132 M. Sakamoto, S. S. Kim, H. Furusho, T. Majima, *Phys. Chem. Chem. Phys.* **2010**, *12*, 365.

133 M. Sakamoto, S. S. Kim, M. Fujitsuka, T. Majima, *J. Phys. Chem. C* **2007**, *111*, 6917.
134 M. Sakamoto, X. Cai, S. S. Kim, M. Fujitsuka, T. Majima, *J. Phys. Chem. A* **2007**, *111*, 223.
135 J. Aizenberg, A. J. Black, G. M. Whitesides, *Nature* **1999**, *398*, 495.
136 J. Aizenberg, *Adv. Mater.* **2004**, *16*, 1295.
137 N. A. J. M. Sommerdijk, G. de With, *Chem. Rev.* **2008**, *108*, 4499.
138 J. A. Lewis, G. M. Gratson, *Mater. Today* **2004**, *7*, 32.
139 K. Jain, M. Klosner, M. Zemel, S. Raghunandan, *Proc. IEEE* **2005**, *93*, 1500.
140 M. Geissler, Y. Xia, *Adv. Mater.* **2004**, *16*, 1249.
141 V. K. Pustovalov, *Chem. Phys.* **2005**, *308*, 103.
142 V. K. Pustovalov, V. A. Babenko, *Laser Phys. Lett.* **2004**, *1*, 516.
143 J. D. Peterson, S. Vyazovkin, C. A. Wight, *J. Phys. Chem. B* **1999**, *103*, 8087.
144 A. S. Kamińska, M. Świątek, *J. Therm. Anal.* **1996**, *46*, 1383.
145 C. Liu, *Adv. Mater.* **2007**, *19*, 3783.
146 G. M. Whitesides, *Nature* **2006**, *442*, 368.
147 C. Sanchez, B. Julián, P. Belleville, M. Popall, *J. Mater. Chem.* **2005**, *15*, 3559.
148 B. A. Grzybowski, R. Haag, N. Bowden, G. M. Whitesides, *Anal. Chem.* **1998**, *70*, 4645.
149 M. J. Williamson, R. M. Tromp, P. M. Vereecken, R. Hull, F. M. Ross, *Nat. Mater.* **2003**, *2*, 532.
150 H. Zheng, R. K. Smith, Y. Jun, C. Kisielowski, U. Dahmen, A. P. Alivisatos, *Science* **2009**, *324*, 1309.

Masanori Sakamoto was born in 1977 in Hiroshima, Japan. He received his B.S. (2000), M.S. (2003) from Kyushu University, and received his Doctorate (2005) from Osaka University under the supervision of Prof. Tetsuro Majima. He worked as a specially appointed assistant professor with Prof. T. Majima in the Institute of Scientific and Industrial Research (SANKEN), Osaka University for four years (2005–2009). From 2009, he has been working in the research group of Prof. T. Teranishi as a research associate in the Graduate School of Pure and Applied Sciences, University of Tsukuba. His current research subject is the synthesis and photochemical properties of metal clusters.

Tetsuro Majima was born in 1952 in Hiroshima, Japan. He received his B.S. and M.S. from the Department of Petroleum Chemistry, Osaka University in 1975 and 1977, respectively, and his Doctorate from the same University under the supervision by Prof. Hiroshi Sakurai and Dr. Chyongjin Pac in 1980. He worked as a research associate with Richard A. Caldwell at the University of Texas at Dallas for two years (1980–1982) before moving to the Institute of Physical and Chemical Research (RIKEN, Japan). He collaborated with Prof. Shigeyoshi Arai and Michio Takami at RIKEN. In 1994 he joined the research group of the late Prof. Setsuo Takamuku as an associate professor in the Institute of Scientific and Industrial Research (SANKEN), Osaka University. He was promoted to full professor in 1997. He is also a Senior Editor of Langmuir since 2007, a WCU adjunct professor, College of Science and Technology, Korea University since 2009, and president of the Japanese Photochemistry Association from 2010. His current research interests include photochemistry of reactive intermediates by multi-beam chemistry, DNA and protein photochemistry, TiO_2 photocatalysts, metal nanoparticles, single-molecule chemistry, energy transfer and electron transfer chemistry, and laser isotope separation.